The opencharm cross section line-shapes

Weiping Wang

November 22, 2017

Abstract

The exclusive opencharm cross sections play crucial role in R value measurement at corresponding energy region. In this energy region, opencharm processes give the dominant contributions to the R value. Therefore, it is necessary that we present a summary of the experimental results of the opencharm cross sections, including the cross section data and corresponding fit. Using this fit, we can create the cross section line-shape data as the input of the generator.

Contents

1 $e^+e^- \to D^{*0}\bar{D}^0$ **3**
- 1.1 the cross section data . . . 3
- 1.2 the phenomenological fit . . . 5

2 $e^+e^- \to D^{*+}D^-$ **6**
- 2.1 the cross section data . . . 6
- 2.2 the phenomenological fit . . . 8

3 $e^+e^- \to D^{*0}\bar{D}^{*0}$ **9**

4 $e^+e^- \to D^{*+}D^{*-}$ **11**

5 $e^+e^- \to D^0\bar{D}^0$ **13**
- 5.1 tag the momentum spectrum . . . 13
- 5.2 tag the recoil mass spectrum . . . 14
- 5.3 the phenomenological fit . . . 16

6 $e^+e^- \to D^+D^-$ **17**
- 6.1 tag the momentum spectrum . . . 17
- 6.2 tag the recoil mass spectrum . . . 18
- 6.3 the phenomenological fit . . . 20

7 $e^+e^- \to D_s^+D_s^-$ **21**
- 7.1 the cross section data . . . 21
- 7.2 the phenomenological fit . . . 24

8 $e^+e^- \to D_s^{*+}D_s^-$ **25**
- 8.1 the cross section data . . . 25
- 8.2 the phenomenological fit . . . 27

9 $e^+e^- \to D_s^{*+}D_s^{*-}$ **28**
- 9.1 the cross section data . . . 28
- 9.2 the phenomenological fit . . . 30

10 $e^+e^- \to D_2^*(2460)\bar{D}$ **31**
- 10.1 BESIII result . . . 31
- 10.2 Belle result . . . 33
- 10.3 Implementing into the generator . . . 33

11 $e^+e^- \to D^0D^{*-}\pi^+$ **36**
- 11.1 the cross section data . . . 36
- 11.2 the phenomenological fit . . . 38
- 11.3 the isospin partners . . . 39

12 $e^+e^- \to \pi^+\pi^- J/\psi$ **40**

13 $e^+e^- \to \pi^+\pi^-\psi(2S)$ **43**

14 $e^+e^- \to \eta J/\psi$ **47**

15 $e^+e^- \to K^+K^- J/\psi$ **48**

16 $e^+e^- \to \pi^+\pi^- h_c$ **50**
- 16.1 the cross section . . . 50
- 16.2 the phenomenological fit . . . 51

17 $e^+e^- \to \Lambda_c^+\bar{\Lambda}_c^-$ **52**

1 $e^+e^- \to D^{*0}\bar{D}^0$

1.1 the cross section data

This process is measured by fitting the momentum spectrum of the D^0, and there is available data from BESIII preliminary measurement, which is listed in Table 1. The CLEO-c collaboration also provided the results in 13 energy points, as shown in blue of Table 1. The Born cross section line-shape measured by BESIII and CLEO-c collaboration are shown in Figure 1.

Table 1: The measured Born cross section of process $e^+e^- \to D^{*0}\bar{D}^0$ by using R-scan data, where the uncertainty is statistical only. The results in blue is cited from CLEO-c results. The abnormal results from BESIII measurement are colored in red. Note that the charge-conjugation mode is included.

$\sqrt{s}$ (GeV)	σ (pb)	$\sqrt{s}$ (GeV)	σ (pb)	$\sqrt{s}$ (GeV)	σ (pb)
3.890	795 ± 81	4.080	1758 ± 137	4.330	840 ± 87
3.895	1133 ± 97	4.090	1416 ± 112	4.340	750 ± 84
3.900	1391 ± 113	4.100	1368 ± 119	4.350	688 ± 83
3.905	1521 ± 125	4.110	1648 ± 130	4.360	797 ± 93
3.910	2022 ± 133	4.120	1166 ± 116	4.370	858 ± 102
3.915	2057 ± 140	4.130	1256 ± 107	4.380	1155 ± 123
3.920	1821 ± 2	4.140	755 ± 89	4.390	765 ± 113
3.925	2102 ± 159	4.145	1121 ± 105	4.395	918 ± 120
3.930	2104 ± 159	4.150	1135 ± 103	4.400	634 ± 111
3.935	1772 ± 62	4.160	1120 ± 100	4.410	822 ± 132
3.940	2881 ± 196	4.170	945 ± 57	4.420	1145 ± 151
3.945	2523 ± 160	4.180	1068 ± 99	4.425	1054 ± 140
3.950	2413 ± 198	4.190	1159 ± 102	4.430	1400 ± 172
3.955	2331 ± 204	4.195	645 ± 70	4.440	743 ± 123
3.960	2896 ± 264	4.200	912 ± 88	4.450	984 ± 142
3.965	2720 ± 237	4.203	923 ± 95	4.460	1167 ± 148
3.970	2542 ± 251	4.206	738 ± 77	4.480	1480 ± 180
3.975	2432 ± 184	4.210	975 ± 92	4.500	1242 ± 165
3.980	4421 ± 293	4.215	616 ± 66	4.520	1166 ± 150
3.985	3121 ± 253	4.220	669 ± 73	4.540	1496 ± 166
3.990	3009 ± 165	4.225	518 ± 63	4.550	1192 ± 153
3.995	3298 ± 178	4.230	464 ± 59	4.560	980 ± 156
4.000	3447 ± 216	4.235	487 ± 64	4.570	958 ± 2
4.005	3493 ± 236	4.240	506 ± 67	4.580	868 ± 141
4.010	4416 ± 279	4.243	637 ± 56	4.590	1689 ± 226
4.012	4082 ± 241	4.245	427 ± 4	3.970	2280 ± 155
4.014	3376 ± 245	4.248	632 ± 73	3.990	2740 ± 182
4.016	4572 ± 275	4.250	651 ± 73	4.010	3320 ± 114
4.018	5058 ± 304	4.255	550 ± 64	4.015	3840 ± 312
4.020	4678 ± 249	4.260	540 ± 68	4.030	3200 ± 213
4.025	3654 ± 199	4.265	564 ± 67	4.060	2230 ± 165
4.030	4146 ± 178	4.270	820 ± 82	4.120	1400 ± 143
4.035	3480 ± 225	4.275	574 ± 69	4.140	1350 ± 110
4.040	3307 ± 215	4.280	638 ± 75	4.160	1252 ± 81
4.050	1912 ± 161	4.285	654 ± 73	4.170	1272 ± 47
4.055	2217 ± 187	4.290	621 ± 65	4.180	1211 ± 101
4.060	1954 ± 238	4.300	474 ± 63	4.200	1030 ± 128
4.065	1967 ± 148	4.310	730 ± 79	4.260	1080 ± 70
4.070	2425 ± 175	4.320	792 ± 79		

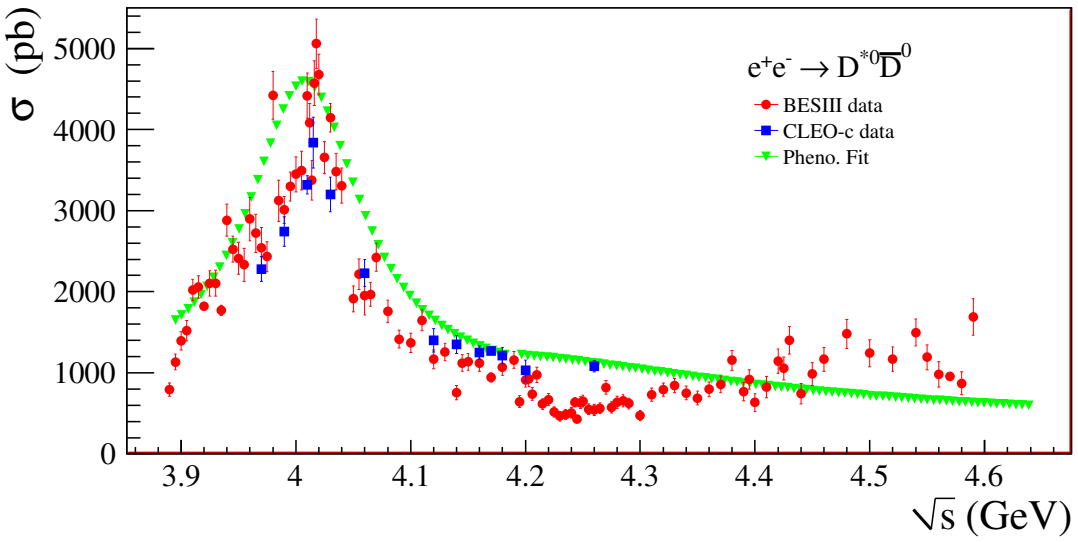

Figure 1: The Born cross section line-shape of process $e^+e^- \to D^{*0}\bar{D}^0$, in which the charge-conjugate mode is included. The phenomenological fit is performed by Prof. Ronggang Ping, which is based on the Belle data.

As for the input of generator, we need a smooth Born cross section line-shape for the process $e^+e^- \to D^{*0}\bar{D}^0$. It is difficult to fit this line-shape shown in Figure 1, since there are several unknown peaks, for example the narrow peak slightly below $\sqrt{s} = 4.0$ GeV. Fortunately, Belle Collaboration has measured the isospin-conjugate process, $e^+e^- \to D^{*+}D^-$, their Born cross section are regarded as the same due to the isospin symmetry, and Prof. Ronggang Ping has performed a phenomenological fit when preparing the inputs for ConExc generator. Figure 2 gives the fit result. Figure 1 also shown the comparison between the BESIII data and the fit results of the Belle data, we can conclude that they are consistent within the uncertainty. Therefore, it is appropriate that we use this fit result as the input for ConExc generator. It should be noticed that all the Born cross section measurements included the charged-conjugate mode, but do not include the isospin-conjugate mode. That is, the $e^+e^- \to D^{*+}D^-$ and $e^+e^- \to D^+D^{*-}$ are not included in the analysis of $e^+e^- \to D^{*0}\bar{D}^0$ and $e^+e^- \to D^0\bar{D}^{*0}$.

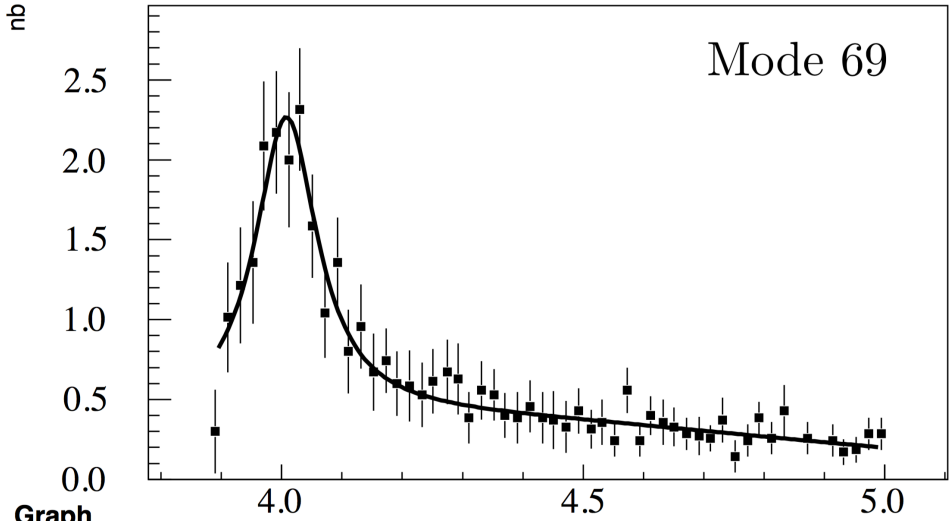

Figure 2: The phenomenological fit of the cross section $e^+e^- \to D^{*+}D^-$, in which the charge conjugate mode is excluded.

1.2 the phenomenological fit

We performed the phenomenological fit of Dr. Gao Zhen data to obtain the smooth and continuum line-shape of $e^+e^- \to D^0\bar{D}^{*0}$. Figure 3 gives the fit result and Figure 4 is corresponding curve.

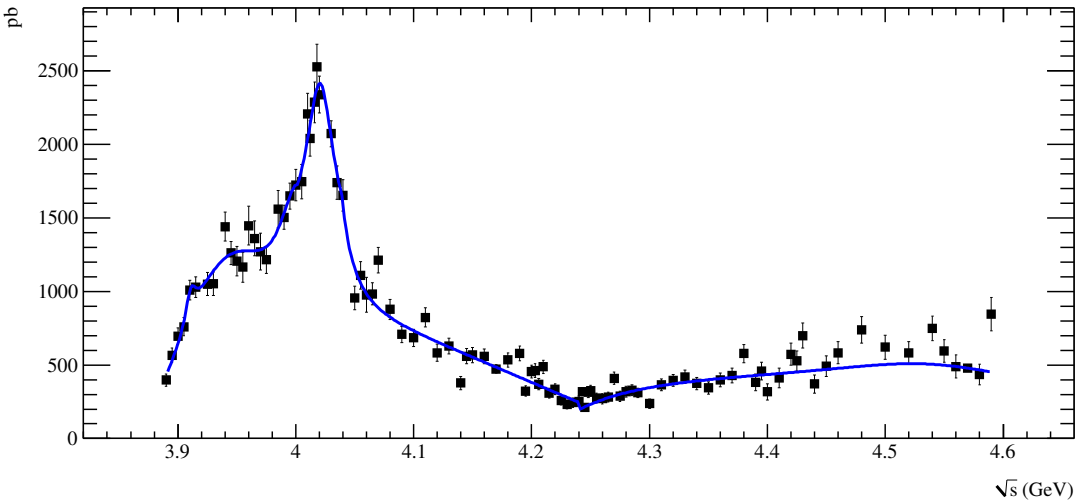

Figure 3: Fit result of Born cross section process $e^+e^- \to D^0\bar{D}^{*0}$ measured by Dr. Gao Zhen.

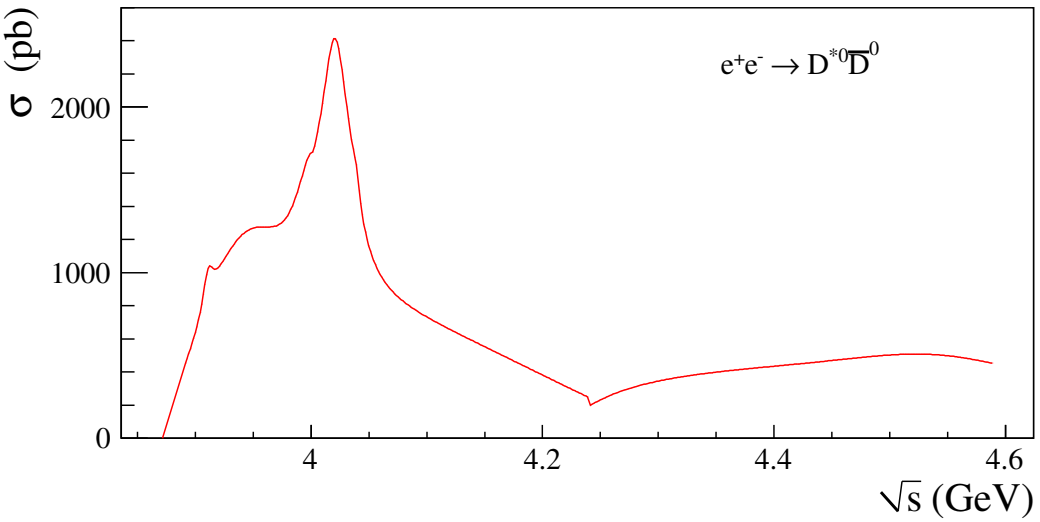

Figure 4: Fit curve of Born cross section process $e^+e^- \to D^0\bar{D}^{*0}$ measured by Dr. Gao Zhen.

Note that the cross section of channel $e^+e^- \to D^0\bar{D}^{*0}$ and $e^+e^- \to \bar{D}^0D^{*0}$ are regarded as the same and assigned to be half of the $e^+e^- \to D^0\bar{D}^{*0} + c.c.$, as we did in this fit procedure. In this fit, we directly discarded a few significantly abnormal data points, they are: 3.92, 3.935, 3.98, 4.014, and 4.025 GeV.

2 $e^+e^- \to D^{*+}D^-$

2.1 the cross section data

This process is measured by fitting the momentum spectrum of the D^0, and there is available data from BESIII preliminary measurement, which is listed in Table 2. The CLEO-c collaboration also provided the results in 13 energy points, as shown in blue of Table 2. The Born cross section line-shape measured by BESIII and CLEO-c collaboration are shown in Figure 5.

Table 2: The measured Born cross section of process $e^+e^- \to D^{*+}D^-$ by using R-scan data, where the uncertainty is statistical only. The results colored in blue is cited from CLEO-c results. The abnormal results from BESIII measurement are marked in red. Note that the charge-conjugation mode is included.

$\sqrt{s}$ (GeV)	σ (pb)	$\sqrt{s}$ (GeV)	σ (pb)	$\sqrt{s}$ (GeV)	σ (pb)
3.890	144 ± 46	4.080	1732 ± 77	4.330	680 ± 49
3.895	58 ± 22	4.090	1215 ± 65	4.340	693 ± 48
3.900	320 ± 34	4.100	1335 ± 72	4.350	640 ± 48
3.905	905 ± 56	4.110	1220 ± 69	4.360	753 ± 54
3.910	1128 ± 64	4.120	1100 ± 62	4.370	705 ± 52
3.915	1320 ± 66	4.130	883 ± 59	4.380	676 ± 54
3.920	1552 ± 75	4.140	1159 ± 66	4.390	969 ± 66
3.925	1764 ± 81	4.145	1202 ± 65	4.395	907 ± 61
3.930	1730 ± 79	4.150	1225 ± 66	4.400	853 ± 66
3.935	2079 ± 85	4.160	990 ± 61	4.410	777 ± 66
3.940	2232 ± 88	4.170	995 ± 41	4.420	966 ± 66
3.945	2267 ± 87	4.180	1138 ± 66	4.425	946 ± 67
3.950	2160 ± 83	4.190	894 ± 58	4.430	858 ± 69
3.955	2453 ± 88	4.195	894 ± 56	4.440	935 ± 68
3.960	2471 ± 85	4.200	963 ± 58	4.450	842 ± 65
3.965	2764 ± 95	4.203	788 ± 57	4.460	813 ± 58
3.970	2539 ± 92	4.206	789 ± 53	4.480	909 ± 66
3.975	2744 ± 93	4.210	619 ± 46	4.500	865 ± 64
3.980	3506 ± 119	4.215	960 ± 61	4.520	825 ± 65
3.985	3007 ± 96	4.220	631 ± 48	4.540	949 ± 70
3.990	2884 ± 96	4.225	613 ± 45	4.550	999 ± 78
3.995	3161 ± 100	4.230	595 ± 42	4.560	959 ± 77
4.000	3568 ± 112	4.235	665 ± 46	4.570	790 ± 74
4.005	3331 ± 107	4.240	511 ± 42	4.580	970 ± 77
4.010	4205 ± 124	4.243	656 ± 51	4.590	1197 ± 121
4.012	3543 ± 113	4.245	736 ± 48	3.970	2230 ± 151
4.014	4305 ± 127	4.248	693 ± 47	3.990	2750 ± 182
4.016	4412 ± 133	4.250	668 ± 46	4.010	3300 ± 173
4.018	4932 ± 136	4.255	712 ± 47	4.015	3703 ± 302
4.020	4922 ± 136	4.260	770 ± 48	4.030	3300 ± 213
4.025	5460 ± 147	4.265	721 ± 48	4.060	2170 ± 161
4.030	4394 ± 82	4.270	704 ± 47	4.120	1560 ± 146
4.035	3563 ± 113	4.275	735 ± 47	4.140	1376 ± 109
4.040	3205 ± 114	4.280	731 ± 48	4.160	1376 ± 83
4.050	2640 ± 103	4.285	709 ± 26	4.170	1285 ± 48
4.055	2272 ± 92	4.290	570 ± 42	4.180	1296 ± 97
4.060	2066 ± 91	4.300	678 ± 41	4.200	1070 ± 121
4.065	1985 ± 88	4.310	748 ± 51	4.260	1022 ± 64
4.070	1632 ± 77	4.320	654 ± 44		

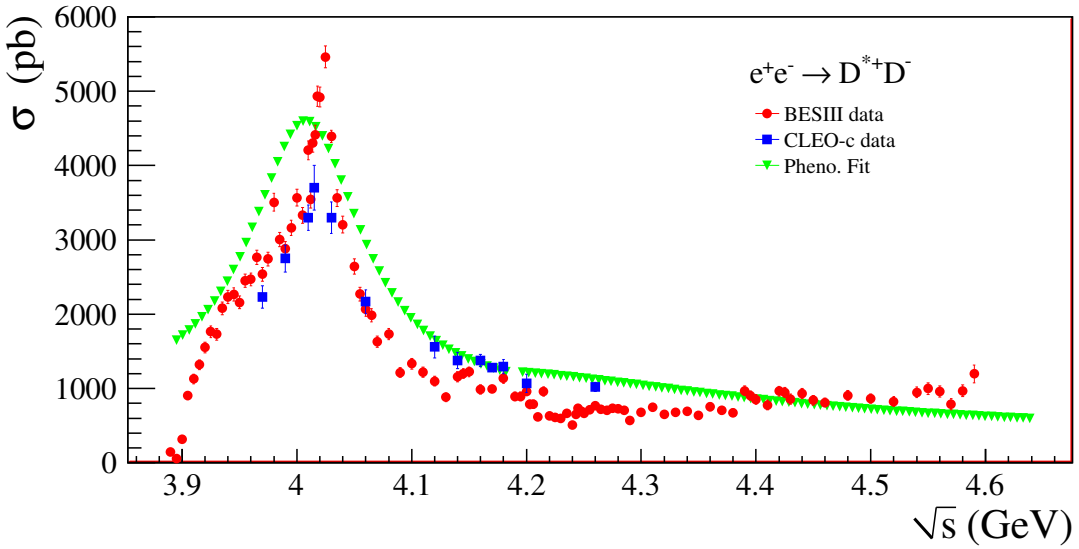

Figure 5: The Born cross section line-shape of process $e^+e^- \to D^{*+}D^-$, in which the charge-conjugate mode is included. The phenomenological fit is performed by Prof. Ronggang Ping, which is based on the Belle data.

Actually, Prof. Ronggang Ping only performed the fit using the $e^+e^- \to D^{*+}D^-$ data of Belle Collaboration as shown in the Figure 2. There is no measured Born cross section result for $e^+e^- \to D^{*0}D^0$ from Belle collaboration. In these two isospin-conjugate modes, their Born cross sections are regarded as the same. Figure 5 shown the comparison between the BESIII data and the fit results of the Belle data, we can conclude that they are consistent within the uncertainty. Therefore, it is OK that we use this fit result as the input for ConExc generator.

2.2 the phenomenological fit

We performed the phenomenological fit of Dr. Gao Zhen data to obtain the smooth and continuum line-shape of $e^+e^- \to D^{*+}D^-$. Figure 6 gives the fit result and Figure 7 is corresponding curve.

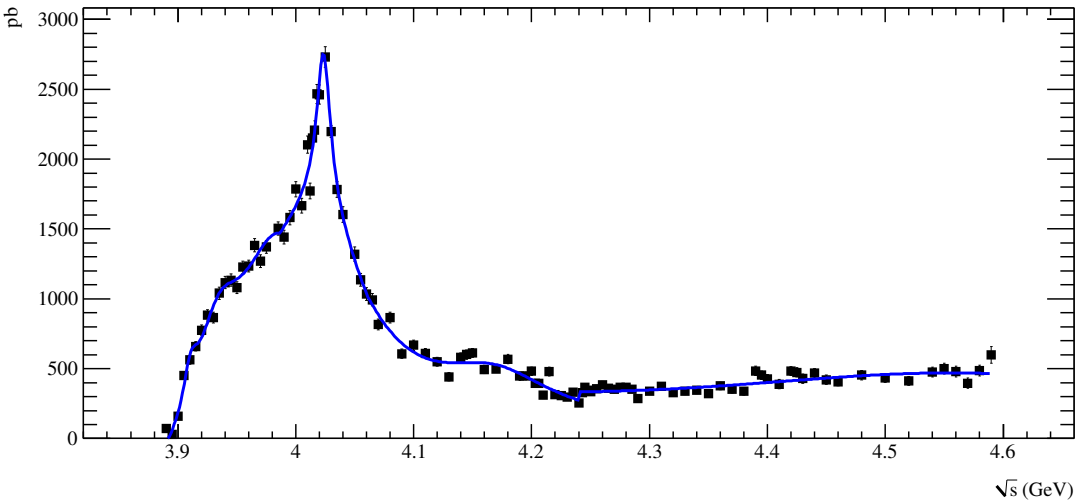

Figure 6: Fit result of Born cross section process $e^+e^- \to D^{*+}D^-$ measured by Dr. Gao Zhen.

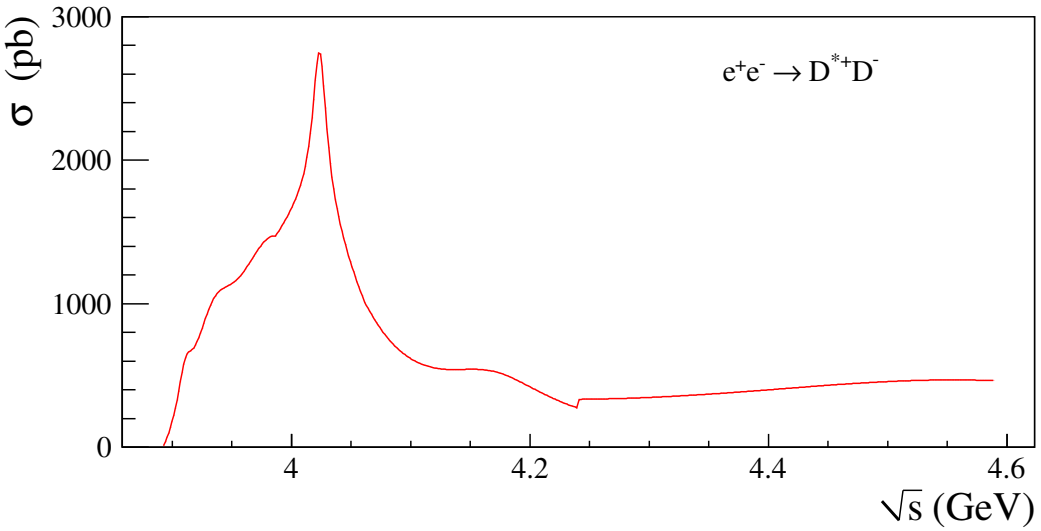

Figure 7: Fit curve of Born cross section process $e^+e^- \to D^{*+}D^-$ measured by Dr. Gao Zhen.

Note that the cross section of channel $e^+e^- \to D^{*+}D^-$ and $e^+e^- \to D^{*-}D^+$ are regarded as the same and assigned to be half of the $e^+e^- \to D^{*+}D^- + c.c.$, as we did in this fit procedure. In this fit, we directly discarded a few significantly abnormal data points, they are: 3.98 GeV.

3 $e^+e^- \to D^{*0}\bar{D}^{*0}$

This process is measured by fitting the momentum spectrum of the D^0, and there is available data from BESIII preliminary measurement, which is listed in Table 3. The CLEO-c collaboration also provided the results in 10 energy points, as shown in blue of Table 3. The Born cross section line-shape measured by BESIII and CLEO-c collaboration are shown in Figure 8.

Table 3: The measured Born cross section of process $e^+e^- \to D^{*0}\bar{D}^{*0}$ by using R-scan data, where the uncertainty is statistical only. The results colored in blue is cited from CLEO-c results. The abnormal results from BESIII measurement are marked in red.

$\sqrt{s}$ (GeV)	σ (pb)	$\sqrt{s}$ (GeV)	σ (pb)	$\sqrt{s}$ (GeV)	σ (pb)
4.016	49 ± 23	4.210	1594 ± 119	4.395	741 ± 104
4.018	114 ± 28	4.215	966 ± 97	4.400	722 ± 116
4.020	587 ± 66	4.220	861 ± 89	4.410	1051 ± 132
4.025	1881 ± 166	4.225	833 ± 93	4.420	837 ± 110
4.030	3429 ± 199	4.230	291 ± 55	4.425	502 ± 105
4.035	3310 ± 199	4.235	313 ± 52	4.430	53 ± 101
4.040	3486 ± 165	4.240	535 ± 78	4.440	92 ± 108
4.050	2666 ± 171	4.243	113 ± 37	4.450	203 ± 100
4.055	3533 ± 191	4.245	146 ± 34	4.460	249 ± 101
4.060	2725 ± 166	4.248	271 ± 48	4.480	484 ± 106
4.065	3092 ± 161	4.250	123 ± 37	4.500	0 ± 18
4.070	3056 ± 165	4.255	149 ± 42	4.520	275 ± 105
4.080	2800 ± 149	4.260	119 ± 39	4.540	109 ± 67
4.090	3168 ± 165	4.265	39 ± 32	4.550	192 ± 101
4.100	2748 ± 153	4.270	354 ± 63	4.560	555 ± 120
4.110	2498 ± 160	4.275	319 ± 59	4.570	83 ± 103
4.120	2286 ± 148	4.280	199 ± 49	4.580	553 ± 138
4.130	2439 ± 160	4.285	486 ± 74	4.590	103 ± 146
4.140	2005 ± 154	4.290	272 ± 42	4.015	213 ± 77
4.145	2521 ± 146	4.300	148 ± 66	4.030	2000 ± 156
4.150	3177 ± 158	4.310	645 ± 88	4.060	2290 ± 171
4.160	2359 ± 144	4.320	875 ± 89	4.120	2550 ± 195
4.170	3624 ± 199	4.330	651 ± 91	4.140	2443 ± 163
4.180	1560 ± 142	4.340	433 ± 83	4.160	2566 ± 147
4.190	1474 ± 131	4.350	299 ± 16	4.170	2363 ± 113
4.195	1817 ± 140	4.360	916 ± 112	4.180	2173 ± 146
4.200	1318 ± 123	4.370	660 ± 101	4.200	1830 ± 163
4.203	1027 ± 125	4.380	876 ± 118	4.260	269 ± 44
4.206	1750 ± 132	4.390	949 ± 120		

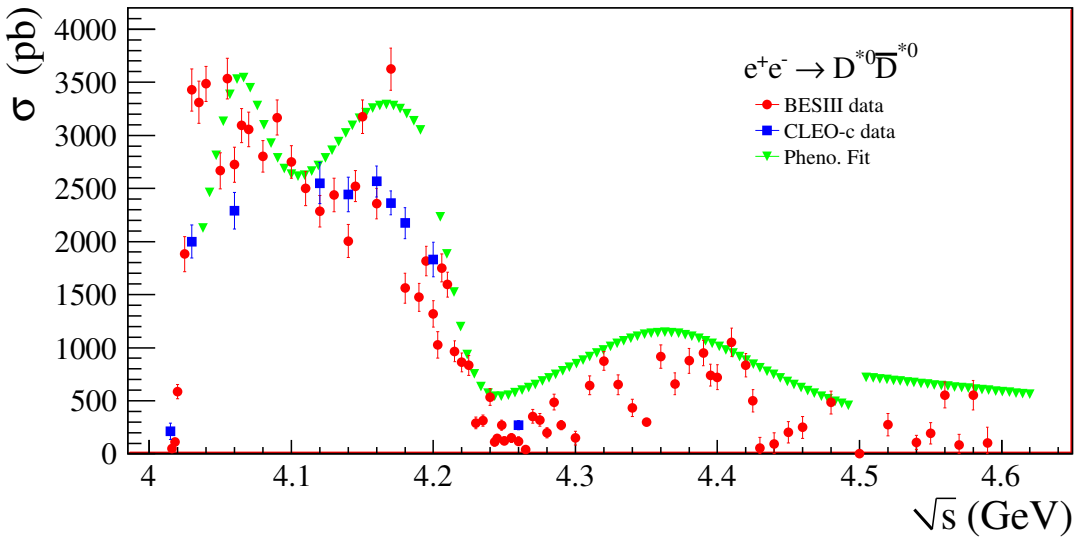

Figure 8: The Born cross section line-shape of process $e^+e^- \to D^{*0}\bar{D}^{*0}$. The phenomenological fit is performed by Prof. Ronggang Ping, which is based on the Belle data.

Similarly, Prof. Ronggang Ping only performed the fit using the $e^+e^- \to D^{*+}D^{*-}$ data of Belle Collaboration as shown in the Figure 9. There is no measured Born cross section result for $e^+e^- \to D^{*0}\bar{D}^{*0}$ from Belle collaboration. In these two isospin-conjugate modes, their Born cross sections are regarded as the same. Figure 8 shown the comparison between the BESIII data and the fit results of the Belle data, we can conclude that they are consistent within the uncertainty. Therefore, it is OK that we use this fit result as the input for ConExc generator.

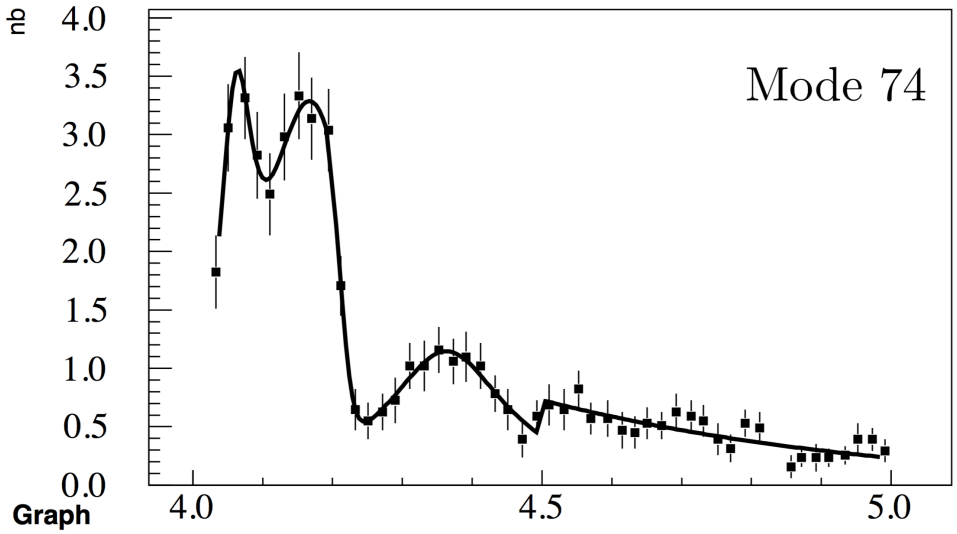

Figure 9: The phenomenological fit of the cross section $e^+e^- \to D^{*+}D^{*-}$, which is measured by Belle collaboration.

4 $e^+e^- \to D^{*+}D^{*-}$

This process is measured by fitting the momentum spectrum of the D^0, and there is available data from BESIII preliminary measurement, which is listed in Table 4. The CLEO-c collaboration also provided the results in 9 energy points, as shown in blue of Table 4. The Born cross section line-shape measured by BESIII and CLEO-c collaboration are shown in Figure 10.

Table 4: The measured Born cross section of process $e^+e^- \to D^{*+}D^{*-}$ by using R-scan data, where the uncertainty is statistical only. The results colored in blue is cited from CLEO-c results. The abnormal results from BESIII measurement are marked in red.

$\sqrt{s}$ (GeV)	σ (pb)	$\sqrt{s}$ (GeV)	σ (pb)	$\sqrt{s}$ (GeV)	σ (pb)
4.030	1359 ± 3	4.220	1318 ± 112	4.395	1377 ± 150
4.035	1995 ± 187	4.225	867 ± 90	4.400	1410 ± 64
4.040	2347 ± 181	4.230	768 ± 81	4.410	825 ± 130
4.050	3062 ± 171	4.235	379 ± 60	4.420	935 ± 131
4.055	2468 ± 168	4.240	288 ± 61	4.425	996 ± 134
4.060	2859 ± 185	4.243	362 ± 62	4.430	1363 ± 164
4.065	3335 ± 218	4.245	292 ± 54	4.440	1140 ± 130
4.070	2930 ± 175	4.248	175 ± 44	4.450	844 ± 116
4.080	3135 ± 172	4.250	230 ± 51	4.460	881 ± 120
4.090	2945 ± 162	4.255	375 ± 62	4.480	372 ± 84
4.100	2567 ± 159	4.260	247 ± 50	4.500	667 ± 113
4.110	3154 ± 179	4.265	419 ± 73	4.520	331 ± 81
4.120	2797 ± 161	4.270	224 ± 52	4.540	813 ± 146
4.130	2765 ± 167	4.275	253 ± 61	4.550	704 ± 142
4.140	3023 ± 173	4.280	472 ± 75	4.560	383 ± 127
4.145	2789 ± 158	4.285	390 ± 32	4.570	448 ± 108
4.150	2396 ± 147	4.290	483 ± 75	4.580	486 ± 110
4.160	2694 ± 155	4.300	692 ± 64	4.590	1284 ± 318
4.170	3009 ± 113	4.310	555 ± 88	4.030	1400 ± 182
4.180	3273 ± 168	4.320	596 ± 86	4.060	2390 ± 249
4.190	2211 ± 144	4.330	956 ± 103	4.120	2280 ± 255
4.195	2481 ± 150	4.340	1244 ± 116	4.140	2556 ± 230
4.200	2328 ± 360	4.350	1036 ± 109	4.160	2479 ± 179
4.203	2077 ± 147	4.360	1143 ± 118	4.170	2357 ± 113
4.206	1531 ± 117	4.370	1330 ± 126	4.180	2145 ± 199
4.210	1604 ± 122	4.380	1216 ± 131	4.200	1564 ± 227
4.215	1500 ± 118	4.390	1307 ± 145	4.260	237 ± 55

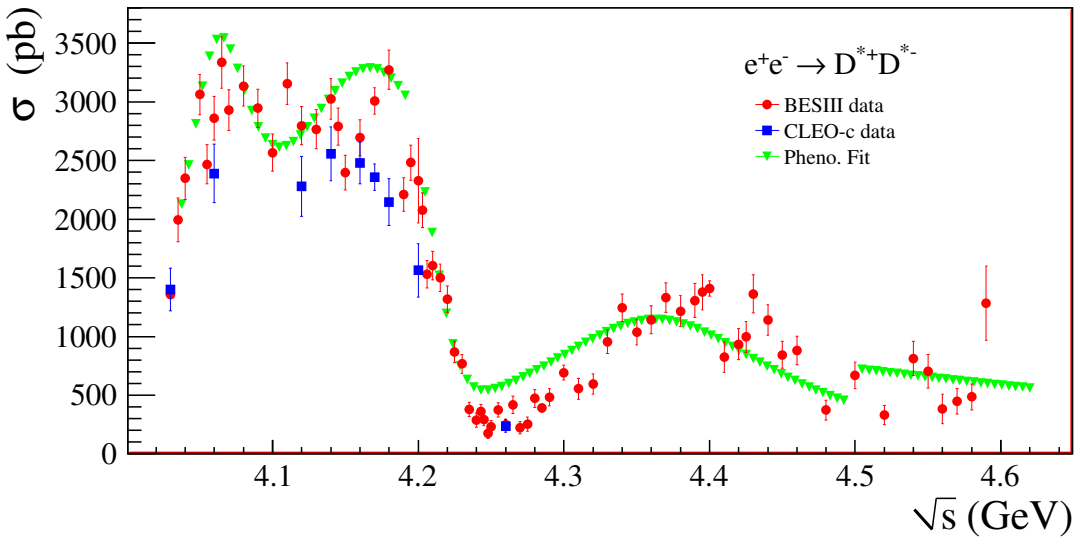

Figure 10: The Born cross section line-shape of process $e^+e^- \to D^{*+}D^{*-}$. The phenomenological fit is performed by Prof. Ronggang Ping, which is based on the Belle data.

The smooth cross section line-shape of process $e^+e^- \to D^{*+}D^{*-}$ is obtained by fitting the Belle data as shown in the Figure 9. Figure 10 shown the comparison between the BESIII data and the fit results of the Belle data, we can conclude that they are consistent within the uncertainty. Therefore, it is OK that we use this fit result as the input for ConExc generator, Figure 11 shows the input curve of channel $e^+e^- \to D^{*0}\bar{D}^{*0}$ and $e^+e^- \to D^{*+}D^{*-}$.

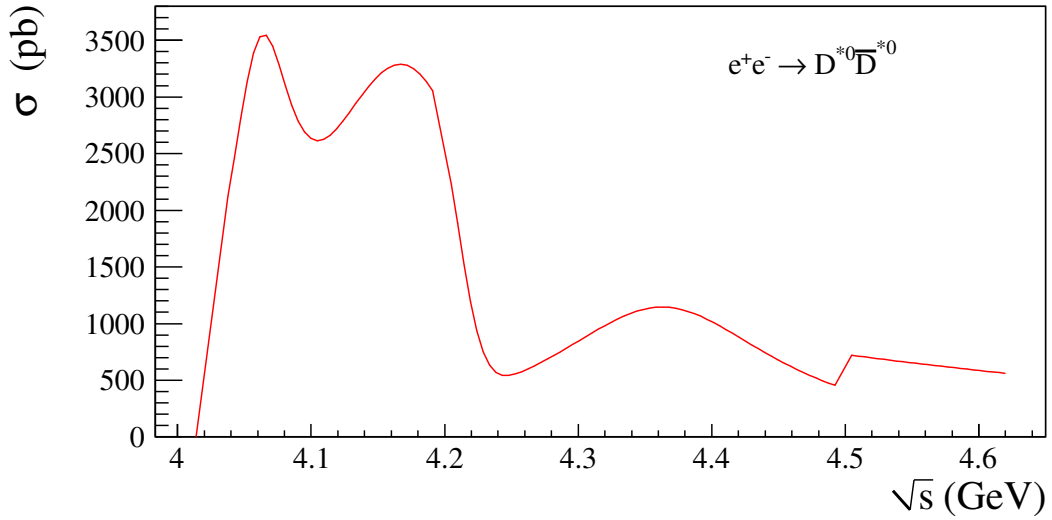

Figure 11: Fit curve of Born cross section process $e^+e^- \to D^{*+}D^{*-}$ measured by Belle collaboration.

Note that the threshold of $D^{*+}D^{*-}$ and $D^{*0}\bar{D}^{*0}$ is different and therefore should be assigned specifically in the generator.

5 $e^+e^- \to D^0\bar{D}^0$

In BESIII collaboration, there are two measured results of $e^+e^- \to D^0\bar{D}^0$ cross section. One is performed by Dr. Gao Zhen with fitting the momentum spectrum of the reconstructed D^0, while another is performed by Dr. Liu Jingyi with fitting the recoiling mass spectrum of tagged D^0. We will present their results separately.

5.1 tag the momentum spectrum

Dr. Gao Zhen measured this processes by fitting the momentum spectrum of the D^0, and there is available data from BESIII preliminary measurement, which is listed in Table 5. The CLEO-c collaboration also provided the results in 13 energy points, as shown in blue of Table 5. The Born cross section line-shape measured by Dr. Gao Zhen and CLEO-c collaboration are shown in Figure 12.

Table 5: Dr. Gao Zhen measured Born cross section of process $e^+e^- \to D^0\bar{D}^0$ by using R-scan data, where the uncertainty is statistical only. The results colored in blue is cited from CLEO-c results. The abnormal results from BESIII measurement are marked in red.

$\sqrt{s}$ (GeV)	σ (pb)	$\sqrt{s}$ (GeV)	σ (pb)	$\sqrt{s}$ (GeV)	σ (pb)	$\sqrt{s}$ (GeV)	σ (pb)
3.850	293 ± 46	4.020	14 ± 11	4.225	178 ± 30	4.425	235 ± 54
3.890	537 ± 56	4.025	244 ± 47	4.230	115 ± 25	4.430	210 ± 52
3.895	405 ± 48	4.030	198 ± 26	4.235	73 ± 21	4.440	240 ± 58
3.900	438 ± 49	4.035	369 ± 53	4.240	16 ± 10	4.450	219 ± 53
3.905	542 ± 57	4.040	410 ± 57	4.243	133 ± 27	4.460	171 ± 46
3.910	372 ± 46	4.050	652 ± 69	4.245	30 ± 1	4.480	190 ± 55
3.915	376 ± 47	4.055	471 ± 54	4.248	66 ± 20	4.500	290 ± 62
3.920	345 ± 1	4.060	420 ± 40	4.250	32 ± 14	4.520	403 ± 77
3.925	361 ± 59	4.065	555 ± 62	4.255	132 ± 27	4.540	203 ± 58
3.930	361 ± 48	4.070	469 ± 55	4.260	24 ± 10	4.550	348 ± 70
3.935	300 ± 25	4.080	560 ± 56	4.265	55 ± 20	4.560	298 ± 85
3.940	288 ± 42	4.090	504 ± 54	4.270	65 ± 21	4.570	162 ± 1
3.945	295 ± 42	4.100	497 ± 57	4.275	37 ± 17	4.580	401 ± 88
3.950	211 ± 36	4.110	376 ± 46	4.280	38 ± 14	4.590	291 ± 102
3.955	128 ± 27	4.120	463 ± 60	4.285	107 ± 25	3.970	86 ± 29
3.960	127 ± 28	4.130	359 ± 43	4.290	61 ± 17	3.990	133 ± 41
3.965	185 ± 35	4.140	281 ± 43	4.300	54 ± 19	4.010	76 ± 25
3.970	124 ± 31	4.145	166 ± 29	4.310	75 ± 22	4.015	0 ± 0
3.975	86 ± 24	4.150	253 ± 39	4.320	53 ± 17	4.030	334 ± 72
3.980	154 ± 37	4.160	85 ± 22	4.330	39 ± 17	4.060	410 ± 74
3.985	42 ± 19	4.170	209 ± 23	4.340	46 ± 20	4.120	303 ± 71
3.990	61 ± 23	4.180	170 ± 32	4.350	70 ± 25	4.140	177 ± 41
3.995	109 ± 28	4.190	218 ± 44	4.360	146 ± 36	4.160	167 ± 29
4.000	18 ± 13	4.195	181 ± 34	4.370	147 ± 37	4.170	177 ± 11
4.005	28 ± 16	4.200	284 ± 41	4.380	219 ± 41	4.180	179 ± 40
4.010	126 ± 33	4.203	102 ± 24	4.390	181 ± 42	4.200	180 ± 56
4.012	47 ± 19	4.206	158 ± 31	4.395	333 ± 56	4.260	86 ± 18
4.014	133 ± 39	4.210	229 ± 39	4.400	189 ± 40		
4.016	40 ± 19	4.215	192 ± 32	4.410	209 ± 51		
4.018	89 ± 30	4.220	131 ± 27	4.420	189 ± 49		

5.2 tag the recoil mass spectrum

Dr. Liu jingyi performed the measurement by fitting the recoil mass spectrum of the tagged D^0, which is reconstructed by $K\pi$. In their analysis, the R-scan as well as the XYZ data is employed. Table 6 listed their cross section results, in which the cross sections obtained by using XYZ data are colored in red. Figure 12 also shows the results from Dr. Liu jingyi for a rough comparison.

Table 6: Dr. Liu jingyi measured Born cross section of process $e^+e^- \to D^0\bar{D}^0$ by using R-scan and XYZ data, where the uncertainty is total uncertainty. The results colored in red is obtained by using XYZ data.

$\sqrt{s}$ (GeV)	σ (pb)	$\sqrt{s}$ (GeV)	σ (pb)	$\sqrt{s}$ (GeV)	σ (pb)
3.80765	0 ± 7	4.065	441 ± 58	4.275	38 ± 24
3.850	189 ± 36	4.070	425 ± 57	4.280	80 ± 26
3.890	438 ± 55	4.080	408 ± 54	4.285	47 ± 24
3.895	421 ± 54	4.08545	441 ± 34	4.290	98 ± 27
3.89624	407 ± 32	4.090	418 ± 55	4.300	54 ± 26
3.900	381 ± 51	4.100	414 ± 56	4.30789	58 ± 12
3.905	483 ± 59	4.110	305 ± 49	4.310	53 ± 27
3.910	366 ± 51	4.120	477 ± 59	4.320	80 ± 24
3.915	478 ± 58	4.130	279 ± 46	4.330	62 ± 25
3.920	350 ± 51	4.140	285 ± 46	4.340	28 ± 21
3.925	338 ± 51	4.145	196 ± 38	4.350	69 ± 26
3.930	341 ± 51	4.150	222 ± 39	4.35826	79 ± 6
3.935	337 ± 49	4.160	157 ± 34	4.360	58 ± 27
3.940	226 ± 42	4.170	192 ± 27	4.370	106 ± 28
3.945	248 ± 43	4.180	198 ± 39	4.380	74 ± 29
3.950	157 ± 37	4.18859	191 ± 20	4.38740	96 ± 13
3.955	179 ± 35	4.190	263 ± 45	4.390	98 ± 30
3.960	135 ± 32	4.195	241 ± 43	4.395	138 ± 36
3.965	239 ± 40	4.200	247 ± 43	4.400	94 ± 32
3.970	147 ± 37	4.203	133 ± 37	4.410	125 ± 37
3.975	149 ± 34	4.206	198 ± 39	4.41558	136 ± 9
3.980	87 ± 30	4.20773	203 ± 19	4.420	75 ± 31
3.985	132 ± 32	4.210	284 ± 45	4.425	117 ± 37
3.990	68 ± 28	4.215	215 ± 40	4.430	128 ± 36
3.995	96 ± 29	4.21713	201 ± 19	4.440	96 ± 31
4.000	51 ± 26	4.220	171 ± 36	4.450	100 ± 33
4.005	87 ± 29	4.225	199 ± 35	4.460	114 ± 27
4.00762	46 ± 4	4.22626	136 ± 9	4.46706	106 ± 10
4.010	76 ± 28	4.230	171 ± 34	4.480	22 ± 24
4.012	51 ± 28	4.235	107 ± 29	4.500	66 ± 27
4.014	45 ± 27	4.240	42 ± 25	4.520	171 ± 33
4.016	91 ± 30	4.24166	53 ± 10	4.52714	75 ± 9
4.018	41 ± 28	4.243	99 ± 26	4.540	70 ± 27
4.020	68 ± 31	4.245	79 ± 26	4.550	87 ± 27
4.025	183 ± 45	4.248	83 ± 25	4.560	37 ± 23
4.030	300 ± 36	4.250	79 ± 25	4.570	26 ± 23
4.035	399 ± 57	4.255	83 ± 28	4.57450	52 ± 11
4.040	343 ± 53	4.25797	79 ± 6	4.580	35 ± 21
4.050	465 ± 63	4.260	45 ± 24	4.590	44 ± 26
4.055	364 ± 54	4.265	130 ± 32	4.59953	59 ± 5
4.060	378 ± 56	4.270	58 ± 26		

Figure 12 gives a comparison between the measurements from Dr. Gao Zhen, Liu Jingyi, and the CLEO-c collaboration, we can conclude that they are consistent within the uncertainty at the c.m.s energy less than 4.4 GeV.

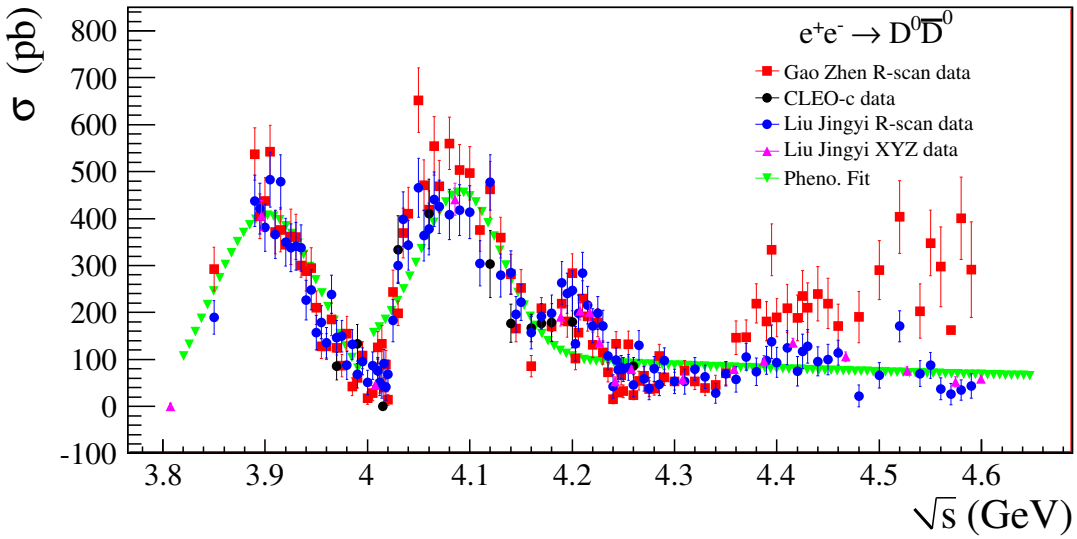

Figure 12: The Born cross section line-shape of process $e^+e^- \to D^0\bar{D}^0$. The phenomenological fit is performed by Prof. Ronggang Ping, which is based on the Belle data.

In order to obtain a smooth line-shape curve, Prof. Ping Ronggang performed a fit using the $e^+e^- \to D^0\bar{D}^0$ data measured by Belle Collaboration, the fit result is shown in the Figure 13. Figure 12 also shows the comparison between the BESIII data and the fit results of the Belle data, we can conclude that they are consistent within the uncertainty, except a systematic deviation around 4.2 GeV. It is neccesary that we use the fit provided by Dr. Liu Jingyi, which is considered this peak around 4.2 GeV, as the input for ConExc generator.

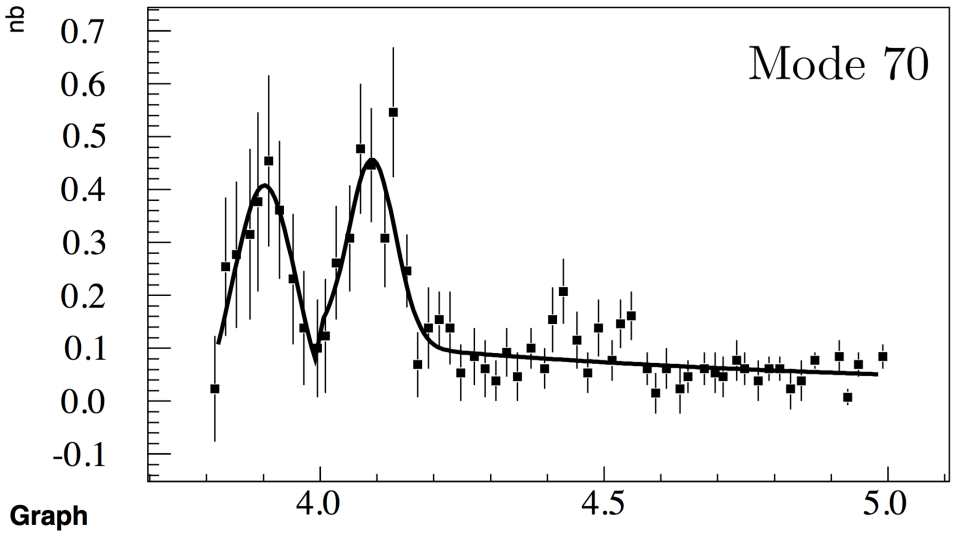

Figure 13: The phenomenological fit of the cross section $e^+e^- \to D^0\bar{D}^0$, which is measured by Belle collaboration.

5.3 the phenomenological fit

We performed the phenomenological fit of Dr. Liu Jingyi data to obtain the smooth and continuum line-shape of $e^+e^- \to D^0\bar{D}^0$. Figure 14 gives the fit result and Figure 15 is corresponding curve.

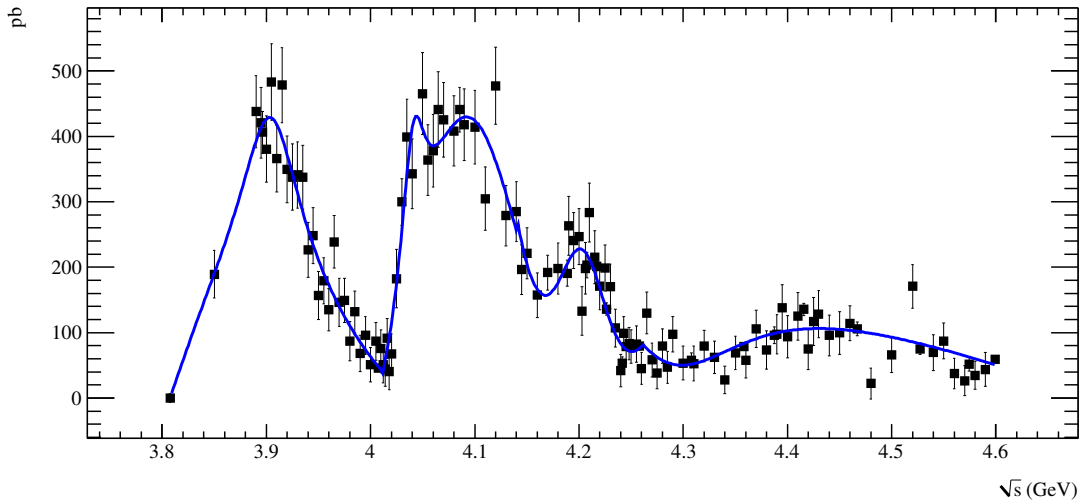

Figure 14: Fit result of Born cross section process $e^+e^- \to D^0\bar{D}^0$ measured by Dr. Liu Jingyi.

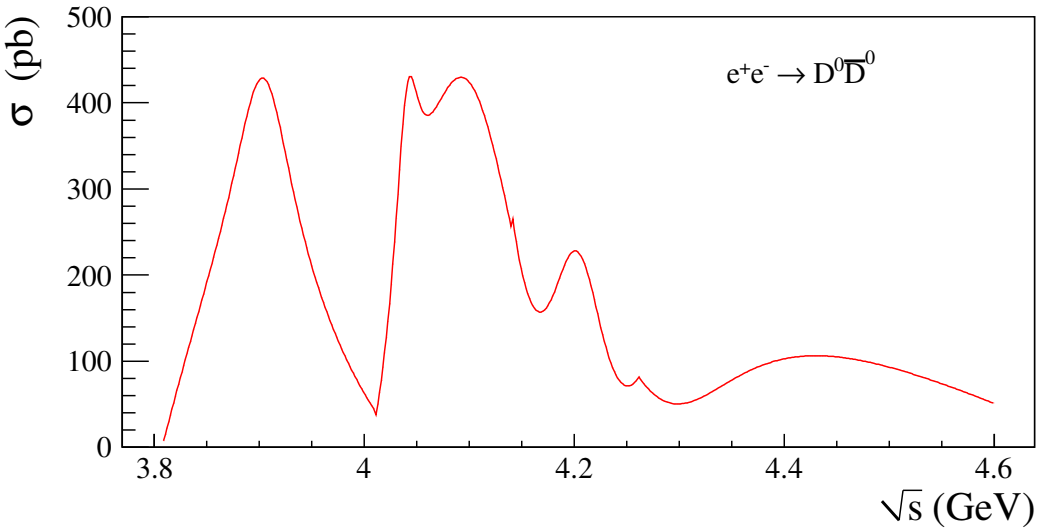

Figure 15: Fit curve of Born cross section process $e^+e^- \to D^0\bar{D}^0$ measured by Dr. Liu Jingyi.

According to this fit, we can find that this curve is better than the one obtained from Belle data, since the resonance around 4.2 GeV is considered in the new fit.

6 $e^+e^- \to D^+D^-$

In BESIII collaboration, there are two measured results of $e^+e^- \to D^+D^-$ cross section. One is performed by Dr. Gao Zhen with fitting the momentum spectrum of the reconstructed D^+, while another is performed by Dr. Liu Jingyi with fitting the recoiling mass spectrum of tagged D^+.

6.1 tag the momentum spectrum

Dr. Gao Zhen measured this processes by fitting the momentum spectrum of the D^+, and there is available data from BESIII preliminary measurement, which is listed in Table 7. The CLEO-c collaboration also provided the results in 13 energy points, as shown in blue of Table 7. The Born cross section line-shape measured by Dr. Gao Zhen and CLEO-c collaboration are shown in Figure 16.

Table 7: The measured Born cross section of process $e^+e^- \to D^+D^-$ by using R-scan data, where the uncertainty is statistical only. The results colored in blue is cited from CLEO-c results. The abnormal results from BESIII measurement are marked in red.

$\sqrt{s}$ (GeV)	σ (pb)	$\sqrt{s}$ (GeV)	σ (pb)	$\sqrt{s}$ (GeV)	σ (pb)	$\sqrt{s}$ (GeV)	σ (pb)
3.850	225 ± 25	4.020	94 ± 20	4.225	185 ± 21	4.425	184 ± 24
3.890	435 ± 33	4.025	180 ± 27	4.230	140 ± 19	4.430	192 ± 26
3.895	442 ± 34	4.030	321 ± 22	4.235	103 ± 17	4.440	132 ± 19
3.900	459 ± 34	4.035	342 ± 32	4.240	68 ± 15	4.450	142 ± 20
3.905	421 ± 32	4.040	379 ± 38	4.243	93 ± 15	4.460	174 ± 20
3.910	430 ± 34	4.050	432 ± 38	4.245	109 ± 17	4.480	136 ± 19
3.915	457 ± 34	4.055	428 ± 36	4.248	107 ± 17	4.500	136 ± 19
3.920	379 ± 32	4.060	453 ± 39	4.250	58 ± 12	4.520	114 ± 18
3.925	381 ± 33	4.065	314 ± 30	4.255	110 ± 18	4.540	105 ± 17
3.930	299 ± 29	4.070	448 ± 36	4.260	86 ± 16	4.550	93 ± 17
3.935	271 ± 28	4.080	462 ± 34	4.265	74 ± 15	4.560	65 ± 14
3.940	244 ± 26	4.090	454 ± 35	4.270	99 ± 17	4.570	81 ± 17
3.945	293 ± 29	4.100	437 ± 34	4.275	101 ± 18	4.580	104 ± 17
3.950	264 ± 27	4.110	361 ± 33	4.280	44 ± 12	4.590	136 ± 28
3.955	254 ± 25	4.120	347 ± 29	4.285	81 ± 8	3.970	137 ± 27
3.960	212 ± 23	4.130	310 ± 29	4.290	70 ± 14	3.990	90 ± 22
3.965	170 ± 22	4.140	201 ± 23	4.300	105 ± 26	4.010	135 ± 23
3.970	140 ± 20	4.145	343 ± 29	4.310	112 ± 18	4.015	38 ± 20
3.975	140 ± 20	4.150	167 ± 20	4.320	114 ± 17	4.030	196 ± 36
3.980	147 ± 26	4.160	176 ± 22	4.330	55 ± 12	4.060	480 ± 59
3.985	149 ± 22	4.170	188 ± 16	4.340	104 ± 19	4.120	310 ± 52
3.990	24 ± 15	4.180	169 ± 22	4.350	74 ± 15	4.140	200 ± 30
3.995	117 ± 20	4.190	176 ± 23	4.360	124 ± 19	4.160	200 ± 23
4.000	20 ± 11	4.195	197 ± 23	4.370	140 ± 20	4.170	182 ± 10
4.005	13 ± 10	4.200	221 ± 24	4.380	130 ± 19	4.180	197 ± 28
4.010	66 ± 18	4.203	206 ± 25	4.390	111 ± 19	4.200	181 ± 37
4.012	95 ± 14	4.206	223 ± 26	4.395	114 ± 18	4.260	94 ± 14
4.014	48 ± 18	4.210	168 ± 22	4.400	182 ± 24		
4.016	11 ± 21	4.215	246 ± 25	4.410	74 ± 17		
4.018	176 ± 30	4.220	178 ± 22	4.420	156 ± 22		

6.2 tag the recoil mass spectrum

Dr. Liu jingyi performed the measurement by fitting the recoil mass spectrum of the tagged D^+, which is reconstructed by $K\pi\pi$. In their analysis, the R-scan as well as the XYZ data is employed. Table 8 listed their cross section results, in which the cross sections obtained by using XYZ data are colored in red. Figure 16 also shows the results from Dr. Liu jingyi for a rough comparison.

Table 8: The measured Born cross section of process $e^+e^- \to D^+D^-$ by using R-scan and XYZ data, where the uncertainty is total uncertainty. The results colored in red is obtained by using XYZ data.

$\sqrt{s}$ (GeV)	σ (pb)	$\sqrt{s}$ (GeV)	σ (pb)	$\sqrt{s}$ (GeV)	σ (pb)
3.80765	1 ± 1	4.065	343 ± 46	4.275	101 ± 19
3.850	239 ± 34	4.070	365 ± 48	4.280	41 ± 14
3.890	435 ± 54	4.080	414 ± 52	4.285	75 ± 16
3.895	443 ± 55	4.08545	400 ± 42	4.290	67 ± 16
3.89624	438 ± 46	4.090	480 ± 59	4.300	83 ± 18
3.900	398 ± 50	4.100	424 ± 53	4.30789	73 ± 10
3.905	397 ± 50	4.110	379 ± 49	4.310	88 ± 18
3.910	411 ± 52	4.120	338 ± 44	4.320	71 ± 16
3.915	429 ± 53	4.130	300 ± 42	4.330	42 ± 13
3.920	358 ± 47	4.140	213 ± 33	4.340	58 ± 15
3.925	373 ± 49	4.145	283 ± 39	4.350	47 ± 15
3.930	286 ± 40	4.150	194 ± 30	4.35826	79 ± 8
3.935	310 ± 42	4.160	167 ± 28	4.360	81 ± 18
3.940	238 ± 35	4.170	195 ± 25	4.370	107 ± 20
3.945	276 ± 38	4.180	187 ± 30	4.380	126 ± 22
3.950	226 ± 33	4.18859	192 ± 22	4.38740	102 ± 12
3.955	146 ± 24	4.190	158 ± 27	4.390	94 ± 19
3.960	213 ± 31	4.195	179 ± 29	4.395	75 ± 17
3.965	190 ± 29	4.200	212 ± 32	4.400	104 ± 21
3.970	159 ± 27	4.203	217 ± 34	4.410	83 ± 20
3.975	141 ± 25	4.206	211 ± 32	4.41558	133 ± 13
3.980	124 ± 24	4.20773	213 ± 23	4.420	123 ± 23
3.985	127 ± 23	4.210	213 ± 31	4.425	142 ± 25
3.990	105 ± 21	4.215	186 ± 29	4.430	150 ± 26
3.995	96 ± 20	4.21713	165 ± 18	4.440	110 ± 21
4.000	79 ± 19	4.220	165 ± 27	4.450	111 ± 21
4.005	49 ± 16	4.225	156 ± 25	4.460	130 ± 22
4.00762	49 ± 5	4.22626	130 ± 13	4.46706	106 ± 12
4.010	45 ± 17	4.230	110 ± 20	4.480	136 ± 22
4.012	49 ± 17	4.235	122 ± 21	4.500	95 ± 18
4.014	8 ± 14	4.240	80 ± 18	4.520	68 ± 15
4.016	32 ± 17	4.24166	93 ± 11	4.52714	73 ± 8
4.018	58 ± 19	4.243	70 ± 17	4.540	78 ± 16
4.020	72 ± 21	4.245	79 ± 17	4.550	59 ± 14
4.025	161 ± 31	4.248	73 ± 17	4.560	67 ± 15
4.030	291 ± 36	4.250	92 ± 18	4.570	36 ± 13
4.035	348 ± 48	4.255	92 ± 18	4.57450	41 ± 6
4.040	357 ± 49	4.25797	82 ± 8	4.580	63 ± 14
4.050	419 ± 54	4.260	79 ± 17	4.590	40 ± 13
4.055	368 ± 49	4.265	78 ± 17	4.59953	68 ± 7
4.060	418 ± 54	4.270	90 ± 18	0.000	0 ± 0

Figure 16 gives a comparison between the measurements from Dr. Gao Zhen, Liu Jingyi, and the CLEO-c collaboration, we can conclude that they are consistent within the uncertainty at the c.m.s energy less than 4.4 GeV.

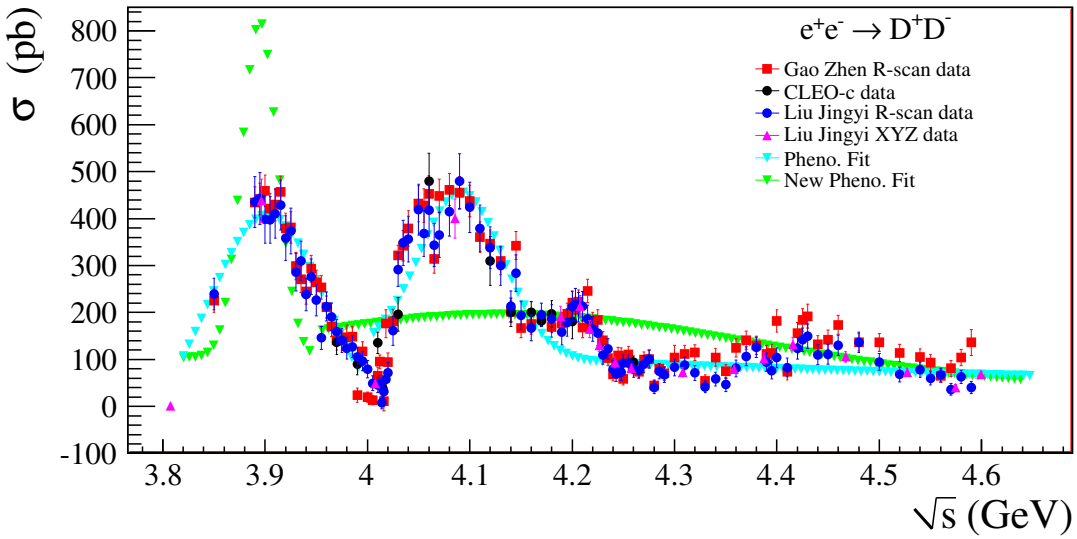

Figure 16: The Born cross section line-shape of process $e^+e^- \to D^+D^-$. The phenomenological fit is performed by Prof. Ronggang Ping, which is based on the Belle data.

The smooth cross section line-shape of process $e^+e^- \to D^+D^-$ is obtained by fitting the Belle data as shown in the Figure 17. Figure 16 shown the comparison between the BESIII data and the fit results of the Belle data. It is obvious that the fit performed here cannot describe the experimental data correctly. Therefore, a new fit should be implemented, at least the fit of $e^+e^- \to D^0\bar{D}^0$ data, shown in Figure 13, should be used.

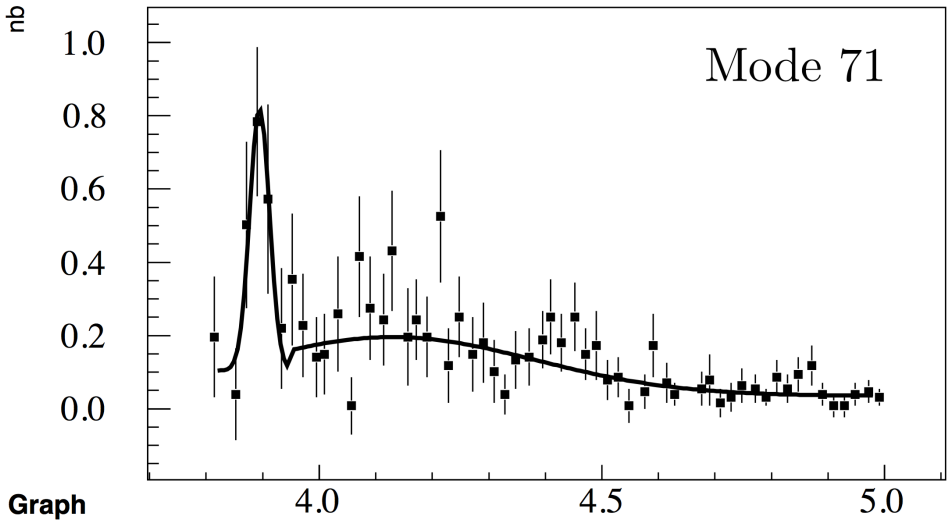

Figure 17: The phenomenological fit of the cross section $e^+e^- \to D^+D^-$, which is measured by Belle collaboration.

6.3 the phenomenological fit

Similarly, we performed the phenomenological fit of Dr. Liu Jingyi data to obtain the smooth and continuum line-shape of $e^+e^- \to D^+D^-$. Figure 18 gives the fit result and Figure 19 is corresponding curve.

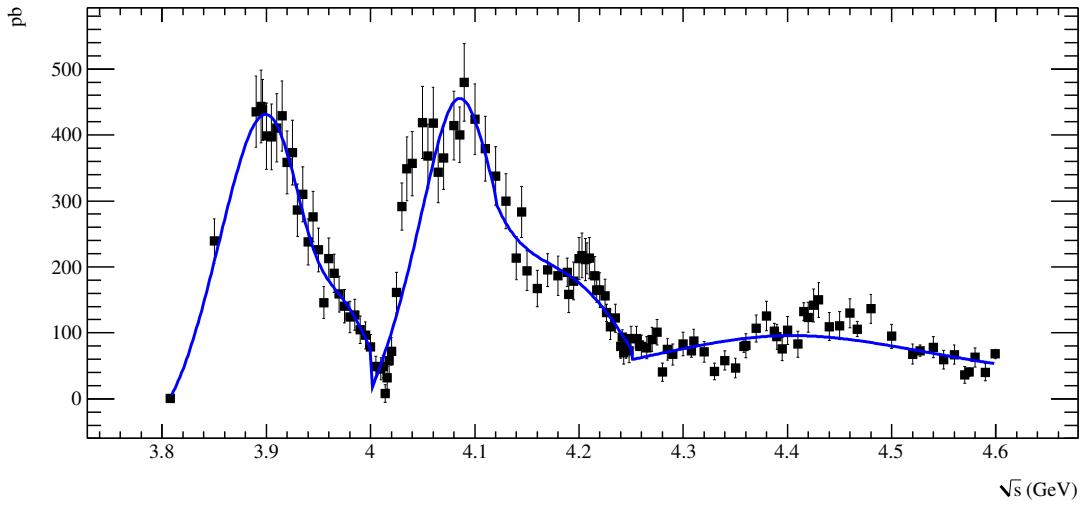

Figure 18: Fit result of Born cross section process $e^+e^- \to D^+D^-$ measured by Dr. Liu Jingyi.

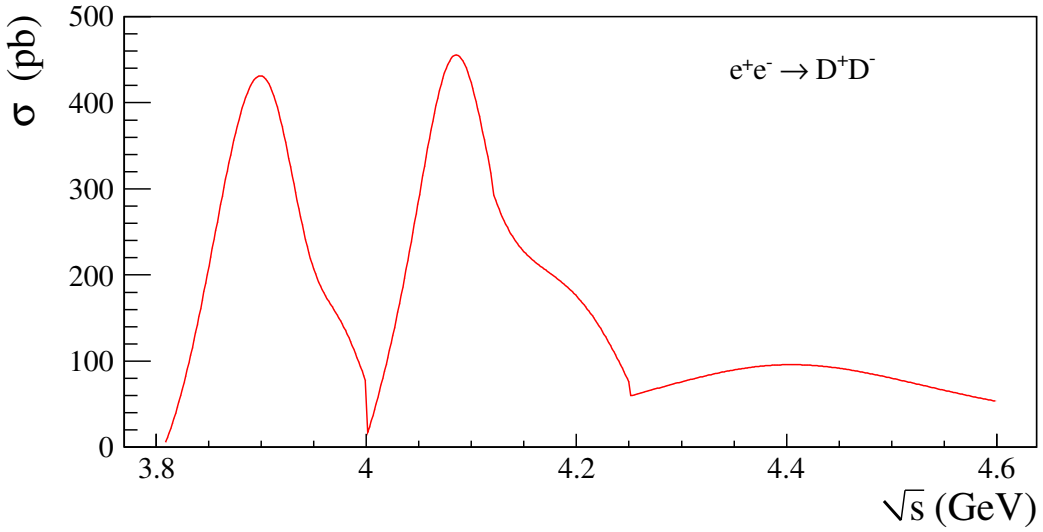

Figure 19: Fit curve of Born cross section process $e^+e^- \to D^+D^-$ measured by Dr. Liu Jingyi.

According to this fit, we can find that this curve is better than the one obtained from Belle data, since the resonance around 4.2 GeV is considered in the new fit.

7 $e^+e^- \to D_s^+D_s^-$

7.1 the cross section data

In BESIII collaboration, there are two independent measurements of this mode. Dr. Li Ke measured the Born cross section by using the R-scan and XYZ data, respectively. In Li Ke's analysis, the simulation is performed using KKMC and EVTGEN. In $e^+e^- \to D_s^+D_s^-$ process, the p-wave VSS model is used to generate the final states of $D_s^+D_s^-$. Table 9 lists the measured results using R-scan and XYZ(colored in red). Figure 21 shows the resulted Born cross section line-shape.

Table 9: Dr. Li Ke measured Born cross section of process $e^+e^- \to D_s^+D_s^-$ by using R-scan data and XYZ data (colored in red), where the uncertainties are total uncertainties.

$\sqrt{s}$ (GeV)	σ (pb)	$\sqrt{s}$ (GeV)	σ (pb)	$\sqrt{s}$ (GeV)	σ (pb)
3.940	0 ± 5	4.150	-17 ± 14	4.390	34 ± 42
3.945	47 ± 31	4.160	60 ± 44	4.395	22 ± 32
3.950	12 ± 16	4.170	37 ± 24	4.400	-11 ± 25
3.955	80 ± 43	4.180	87 ± 41	4.410	55 ± 43
3.960	63 ± 39	4.190	47 ± 37	4.420	79 ± 49
3.965	25 ± 28	4.195	43 ± 40	4.425	26 ± 30
3.970	84 ± 46	4.200	81 ± 50	4.430	68 ± 49
3.975	84 ± 47	4.203	88 ± 54	4.440	51 ± 38
3.980	164 ± 64	4.206	146 ± 67	4.450	4 ± 34
3.985	143 ± 60	4.210	38 ± 41	4.460	85 ± 61
3.990	75 ± 45	4.215	-10 ± 28	4.480	29 ± 31
3.995	224 ± 74	4.220	30 ± 38	4.500	26 ± 31
4.000	155 ± 64	4.225	-1 ± 14	4.520	23 ± 29
4.005	266 ± 84	4.230	6 ± 25	4.540	68 ± 39
4.010	300 ± 91	4.235	41 ± 48	4.550	36 ± 29
4.012	391 ± 103	4.240	28 ± 33	4.560	9 ± 22
4.014	418 ± 107	4.243	40 ± 35	4.570	40 ± 32
4.016	491 ± 115	4.245	0 ± 35	4.580	3 ± 21
4.018	501 ± 109	4.248	25 ± 45	4.590	6 ± 20
4.020	430 ± 87	4.250	43 ± 39	4.00762	335 ± 12
4.025	340 ± 91	4.255	89 ± 51	4.08550	47 ± 14
4.030	353 ± 57	4.260	49 ± 44	4.18860	46 ± 17
4.035	411 ± 97	4.265	117 ± 55	4.20770	43 ± 15
4.040	254 ± 79	4.270	51 ± 39	4.21710	25 ± 12
4.050	80 ± 50	4.275	57 ± 38	4.22626	15 ± 2
4.055	22 ± 33	4.280	45 ± 38	4.24160	41 ± 15
4.060	139 ± 67	4.285	38 ± 32	4.25797	50 ± 4
4.065	58 ± 43	4.290	91 ± 42	4.30790	46 ± 12
4.070	79 ± 39	4.300	46 ± 30	4.35820	35 ± 2
4.080	92 ± 50	4.310	53 ± 17	4.38740	30 ± 12
4.090	75 ± 45	4.320	48 ± 32	4.41558	35 ± 3
4.100	29 ± 37	4.330	16 ± 23	4.46706	35 ± 8
4.110	15 ± 28	4.340	21 ± 30	4.52714	21 ± 6
4.120	33 ± 39	4.350	25 ± 34	4.57450	15 ± 12
4.130	-6 ± 20	4.360	102 ± 45	4.59953	22 ± 3
4.140	8 ± 30	4.370	19 ± 33		
4.145	38 ± 35	4.380	30 ± 36		

Dr. Gao Zhen also measured the cross section of process $e^+e^- \to D_s^+D_s^-$ by fitting the momentum spectrum of D_s^+, as listed in Table 10. There is also the published Born cross section result from CLEO-c collaboration (colored in blue).

Belle collaboration also measured the dressed cross section of process $e^+e^- \to D_s^+D_s^-$, as shown in Figure 20. We can find that their result is almost consistent with that of BESIII.

Table 10: Dr. Gao Zhen measured Born cross section of process $e^+e^- \to D_s^+ D_s^-$ by using R-scan data and the cross section published by CLEO-c collaboration (colored in blue). The results of Dr Gao Zhen only included the statistic uncertainty, while that of CLEO-c is total uncertainty.

$\sqrt{s}$ (GeV)	σ (pb)	$\sqrt{s}$ (GeV)	σ (pb)	$\sqrt{s}$ (GeV)	σ (pb)
3.945	28 ± 13	4.145	0 ± 16	4.360	76 ± 31
3.950	20 ± 12	4.150	0 ± 21	4.370	98 ± 33
3.955	84 ± 28	4.160	60 ± 34	4.380	87 ± 37
3.960	38 ± 17	4.170	117 ± 27	4.390	52 ± 34
3.965	99 ± 27	4.180	47 ± 29	4.395	75 ± 42
3.970	152 ± 40	4.190	92 ± 45	4.400	63 ± 36
3.975	185 ± 37	4.195	119 ± 42	4.410	52 ± 36
3.980	281 ± 53	4.200	27 ± 22	4.420	117 ± 38
3.985	174 ± 37	4.203	38 ± 31	4.425	97 ± 37
3.990	215 ± 39	4.206	63 ± 34	4.430	142 ± 48
3.995	220 ± 45	4.210	5 ± 78	4.440	80 ± 38
4.000	194 ± 40	4.215	17 ± 10	4.450	67 ± 34
4.005	332 ± 53	4.220	76 ± 31	4.460	104 ± 0
4.010	365 ± 57	4.225	0 ± 26	4.480	171 ± 40
4.012	369 ± 54	4.230	0 ± 12	4.500	2 ± 95
4.014	566 ± 71	4.235	0 ± 26	4.520	47 ± 32
4.016	639 ± 70	4.240	55 ± 25	4.540	45 ± 26
4.018	550 ± 67	4.243	75 ± 40	4.550	78 ± 32
4.020	708 ± 74	4.245	69 ± 29	4.560	53 ± 34
4.025	587 ± 68	4.248	12 ± 37	4.570	77 ± 32
4.030	490 ± 45	4.250	73 ± 32	4.580	64 ± 38
4.035	637 ± 71	4.255	54 ± 24	4.590	85 ± 65
4.040	363 ± 62	4.260	50 ± 23	3.970	102 ± 27
4.050	114 ± 41	4.265	86 ± 33	3.990	133 ± 32
4.055	203 ± 53	4.270	13 ± 18	4.010	269 ± 34
4.060	238 ± 59	4.275	150 ± 46	4.015	250 ± 61
4.065	86 ± 33	4.280	47 ± 24	4.030	174 ± 37
4.070	124 ± 43	4.285	138 ± 35	4.060	51 ± 28
4.080	57 ± 29	4.290	136 ± 38	4.120	26 ± 26
4.090	228 ± 56	4.300	17 ± 38	4.140	25 ± 20
4.100	38 ± 27	4.310	86 ± 39	4.160	0 ± 0
4.110	137 ± 46	4.320	111 ± 37	4.170	34 ± 4
4.120	95 ± 45	4.330	101 ± 42	4.180	7 ± 16
4.130	13 ± 35	4.340	102 ± 39	4.200	15 ± 22
4.140	152 ± 52	4.350	187 ± 44	4.260	47 ± 22

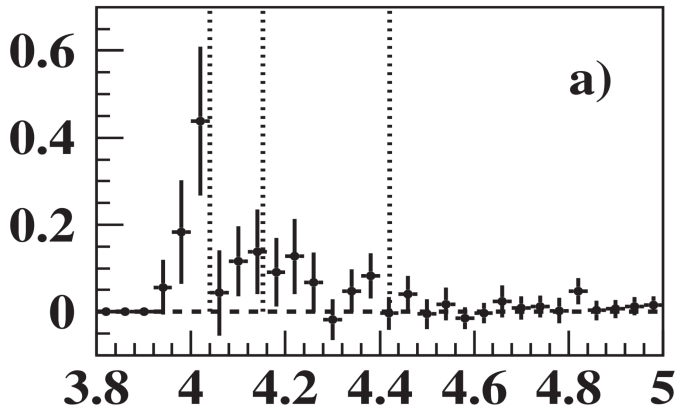

Figure 20: The dressed cross section of $e^+e^- \to D_s^+ D_s^-$, which is measured by Belle collaboration.

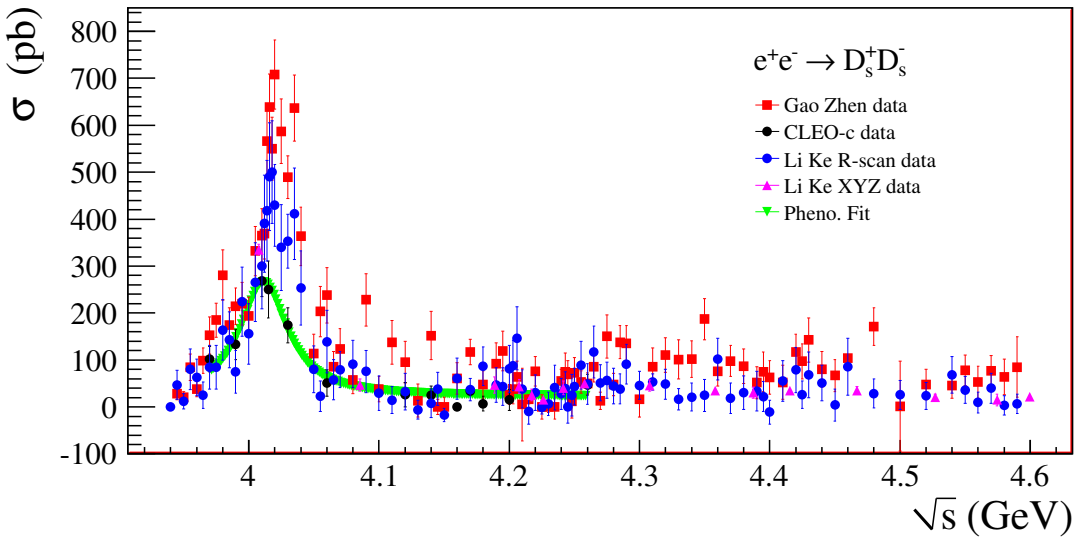

Figure 21: The Born cross section line-shape of process $e^+e^- \to D_s^+ D_s^-$.

Figure 21 shows the cross section line-shape of process $e^+e^- \to D_s^+ D_s^-$, measured by Dr. Gao Zhen, Dr. Li Ke, and CLEO-c collaboration. The phenomenological performed by Prof. Ronggang Ping is also shown in Figure 21 to present a comparison. Actually, according to the comparison, one can find this phenomenological fit is performed based on the CLEO-c data, as shown in Figure 22. According to the fit result, we find that the fit can hardly describe the data provided by Dr. Gao Zhen and Dr. Li Ke, and at the higher energy points, there is no fit results. Therefore, a new fit strategy is need to achieve a better describe of the experimental data.

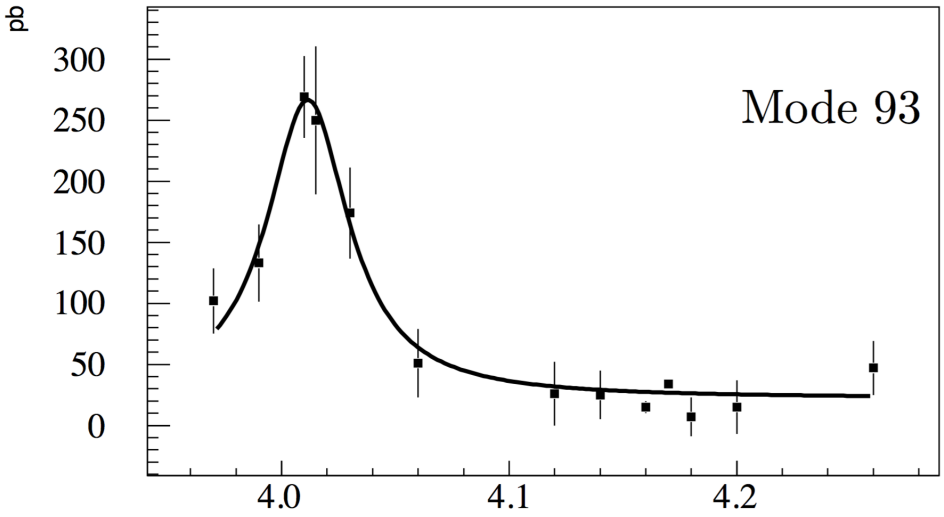

Figure 22: The phenomenological fit of the cross section $e^+e^- \to D_s^+ D_s^-$, which is measured by CLEO-c collaboration.

7.2 the phenomenological fit

We performed the phenomenological fit of Dr. Li Ke data to obtain the smooth and continuum line-shape of $e^+e^- \to D_s^+ D_s^-$. Figure 23 gives the fit result and Figure 24 is corresponding curve.

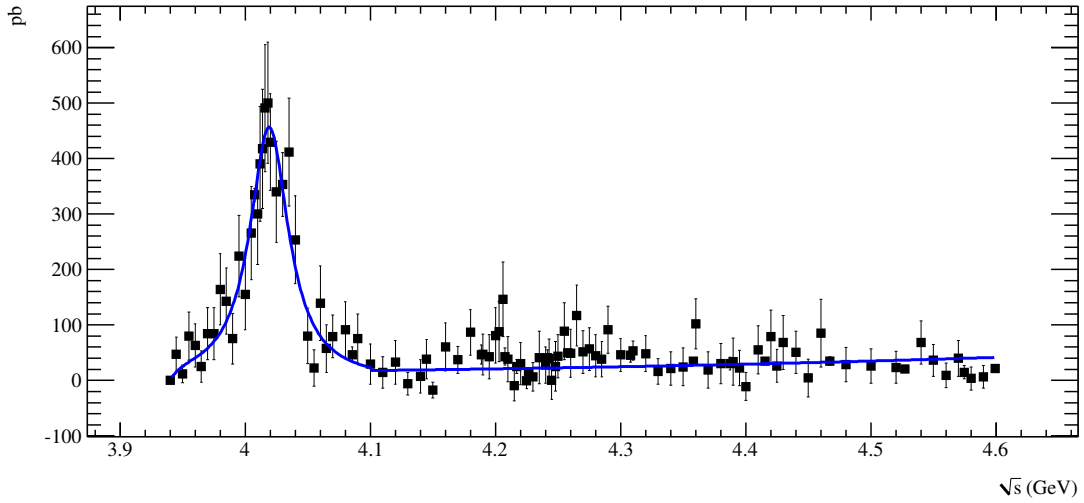

Figure 23: Fit result of Born cross section process $e^+e^- \to D_s^+ D_s^-$ measured by Dr. Li Ke.

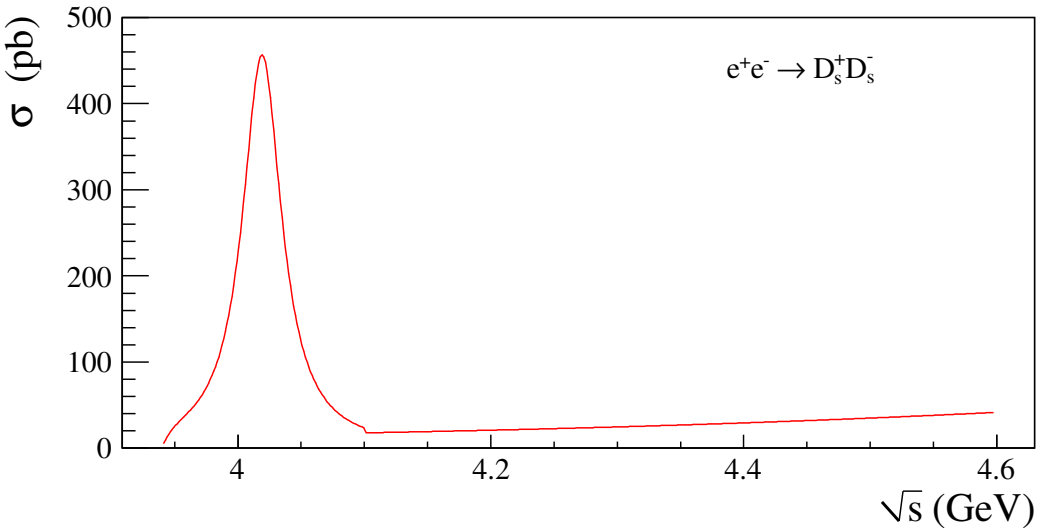

Figure 24: Fit curve of Born cross section process $e^+e^- \to D_s^+ D_s^-$ measured by Dr. Li Ke.

8 $e^+e^- \to D_s^{*+}D_s^-$

8.1 the cross section data

This process is measured by fitting the momentum spectrum of the D_s^+, and there is available data from BESIII preliminary measurement, which is listed in Table 11. The CLEO-c collaboration also provided the results in 7 energy points, as shown in blue of Table 11. The Born cross section line-shape measured by BESIII and CLEO-c collaboration are shown in Figure 26.

Table 11: The measured Born cross section of process $e^+e^- \to D_s^{*+}D_s^-$ by using R-scan data, where the uncertainty is statistical only. The results colored in blue is cited from CLEO-c results, whose uncertainty is total uncertainty. Note that the charge-conjugation mode $e^+e^- \to D_s^+D_s^{*-}$ is included.

$\sqrt{s}$ (GeV)	σ (pb)	$\sqrt{s}$ (GeV)	σ (pb)	$\sqrt{s}$ (GeV)	σ (pb)
4.090	89 ± 30	4.245	213 ± 53	4.420	405 ± 82
4.100	315 ± 52	4.248	105 ± 40	4.425	548 ± 95
4.110	388 ± 68	4.250	138 ± 54	4.430	858 ± 129
4.120	765 ± 78	4.255	84 ± 33	4.440	189 ± 72
4.130	718 ± 81	4.260	120 ± 40	4.450	438 ± 96
4.140	1107 ± 96	4.265	38 ± 25	4.460	358 ± 0
4.145	1115 ± 95	4.270	78 ± 34	4.480	288 ± 75
4.150	1314 ± 97	4.275	17 ± 23	4.500	313 ± 88
4.160	1546 ± 107	4.280	98 ± 39	4.520	309 ± 87
4.170	1265 ± 65	4.285	277 ± 61	4.540	147 ± 60
4.180	1365 ± 108	4.290	42 ± 29	4.550	216 ± 76
4.190	963 ± 95	4.300	319 ± 75	4.560	552 ± 109
4.195	1326 ± 109	4.310	79 ± 71	4.570	333 ± 80
4.200	962 ± 93	4.320	285 ± 69	4.580	381 ± 88
4.203	960 ± 104	4.330	309 ± 88	4.590	241 ± 117
4.206	1014 ± 99	4.340	302 ± 77	4.120	478 ± 69
4.210	1331 ± 103	4.350	472 ± 88	4.140	684 ± 69
4.215	664 ± 77	4.360	502 ± 79	4.160	905 ± 49
4.220	865 ± 94	4.370	804 ± 99	4.170	916 ± 50
4.225	730 ± 80	4.380	301 ± 68	4.180	889 ± 75
4.230	552 ± 69	4.390	535 ± 96	4.200	812 ± 93
4.235	504 ± 68	4.395	620 ± 104	4.260	34 ± 9
4.240	232 ± 55	4.400	787 ± 105		
4.243	135 ± 39	4.410	469 ± 89		

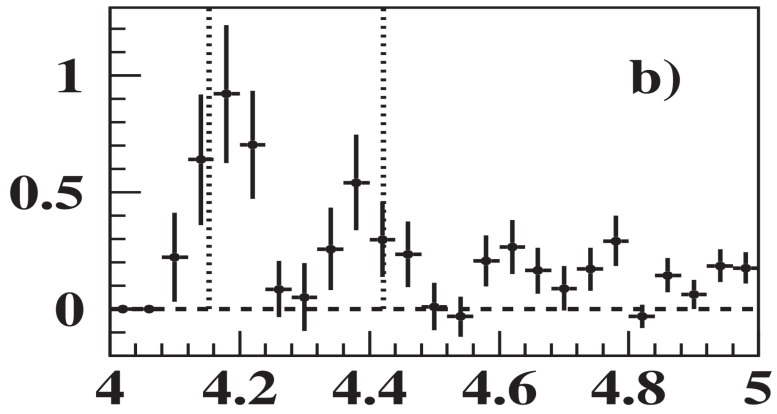

Figure 25: The dressed cross section of $e^+e^- \to D_s^{*+}D_s^-$, which is measured by Belle collaboration.

Belle collaboration also measured the dressed cross section of process $e^+e^- \to D_s^{*+}D_s^-$, as shown in Figure 25. We can find that their result is almost consistent with that of BESIII.

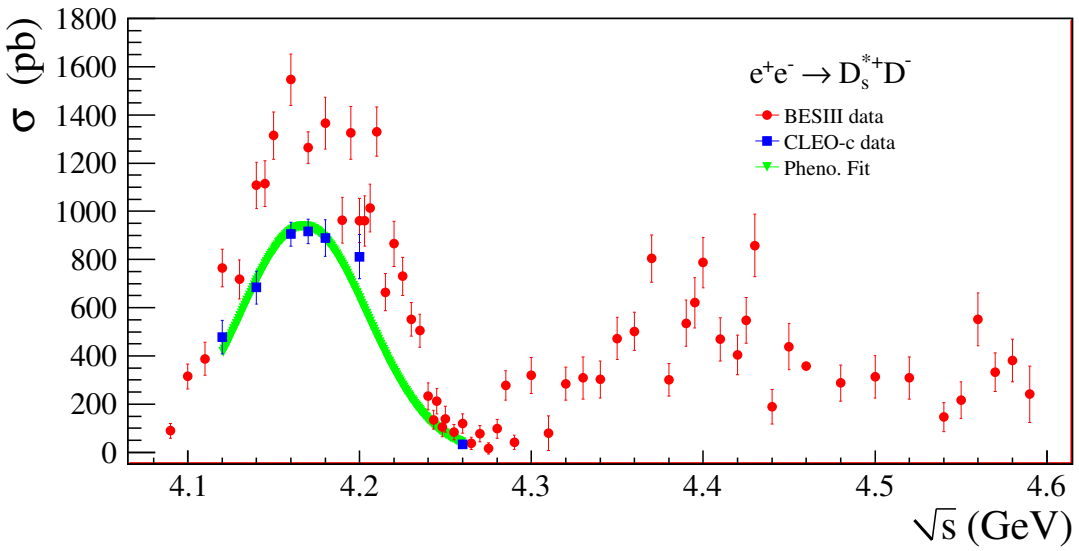

Figure 26: The Born cross section line-shape of process $e^+e^- \to D_s^{*+}D_s^-$. The phenomenological fit is performed by Prof. Ronggang Ping, which is based on the Belle data.

The smooth cross section line-shape of process $e^+e^- \to D_s^{*+}D_s^-$ is obtained by fitting the CLEO-c data as shown in the Figure 27. Figure 26 shown the comparison between the BESIII data and the fit results of the CLEO-c data, we can find that the fit can hardly describe the BESIII data. Therefore, it is needed that we create a new fit to provide the input for ConExc generator.

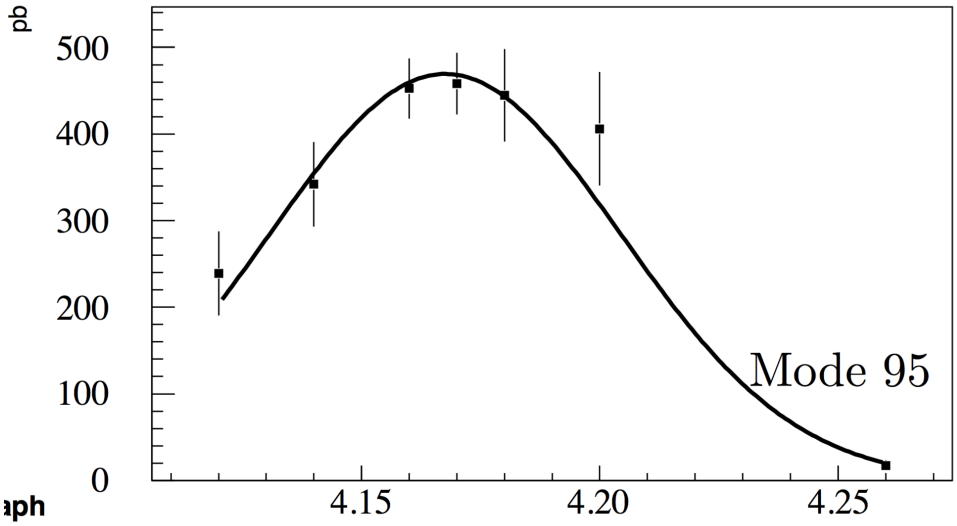

Figure 27: The phenomenological fit of the cross section $e^+e^- \to D_s^{*+}D_s^-$, which is measured by CLEO-c collaboration.

8.2 the phenomenological fit

Since neither the BESIII data nor the CLEO data is consistent with the cross section measured by Belle collaboration, before performing a phenomenological fit, we combined the data from BESIII (measured by Dr. Gao Zhen) and CLEO collaborations. That is, for the energy point whose cross section is measured by both the two collaborations, we use the arithmetical average value of these two cross section data, while for those points where no CLEO data available we only use BESIII data. For the combined data points, their total uncertainties are obtained by assuming the measurements from BESIII and CLEO are uncorrelated.

We performed the phenomenological fit of combined data to obtain the smooth and continuum line-shape of $e^+e^- \to D_s^{*+}D_s^-$. Figure 28 gives the fit result and Figure 29 is corresponding curve.

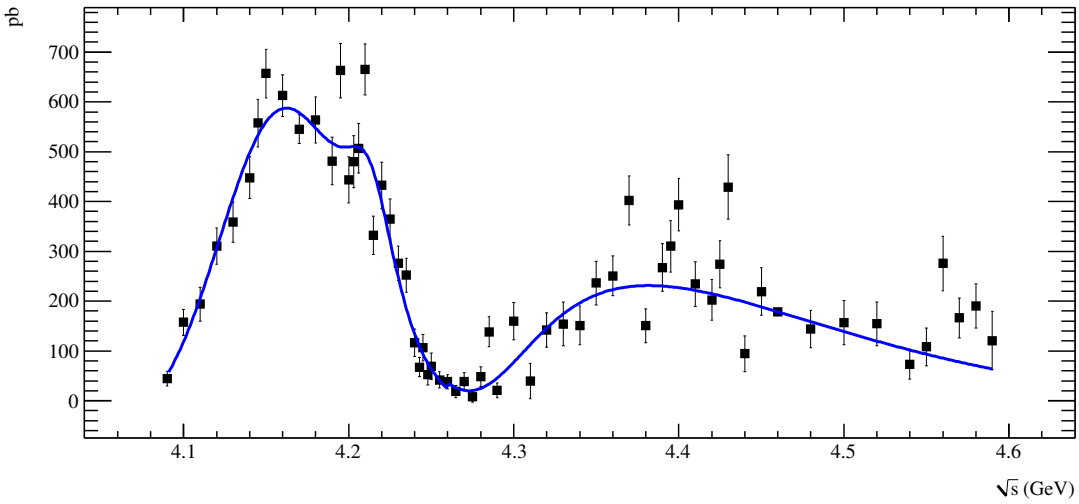

Figure 28: Fit result of Born cross section process $e^+e^- \to D_s^{*+}D_s^-$ measured by Dr. Gao Zhen.

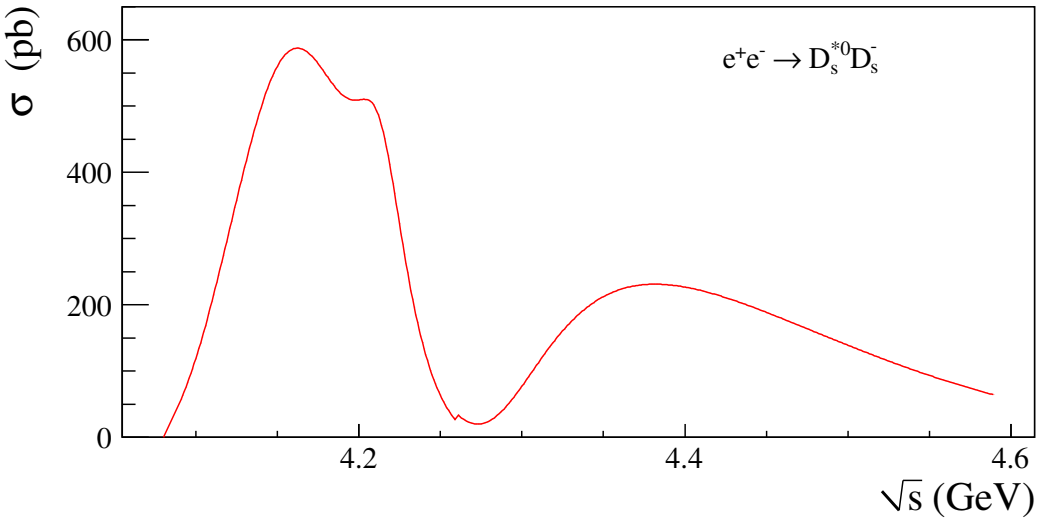

Figure 29: Fit curve of Born cross section process $e^+e^- \to D_s^{*+}D_s^-$ measured by Dr. Gao Zhen.

Note that the cross section channel $e^+e^- \to D_s^{*+}D_s^-$ and $e^+e^- \to D_s^{*-}D_s^+$ are regarded as the same and assigned to be half of the $e^+e^- \to D_s^{*+}D_s^- + c.c.$, as we did in this fit procedure.

9 $e^+e^- \to D_s^{*+}D_s^{*-}$

9.1 the cross section data

There are two measurements of this channel in BESIII collaboration. One is performed by Dr. Gao Zhen, in which the number of signal events is obtained by fitting the momentum spectrum of D_s^+. The results of Dr. Gao Zhen is listed in Table 12. Another is provided by Dr. Wang Liangliang via fitting the invariant mass spectrum of the D_s^{*+}. Dr. Wang provide the results with R-scan and XYZ data, respectively. The corresponding results are listed in Table 13. The CLEO-c collaboration also provided the results at 1 energy points, as shown in blue of Table 12.

Table 12: Dr. Gao Zhen measured Born cross section of process $e^+e^- \to D_s^{*+}D_s^{*-}$ by using R-scan data, where the uncertainty is statistical only. The results colored in blue is cited from CLEO-c results, whose uncertainty is total uncertainty.

$\sqrt{s}$ (GeV)	σ (pb)	$\sqrt{s}$ (GeV)	σ (pb)	$\sqrt{s}$ (GeV)	σ (pb)
4.235	308 ± 42	4.310	393 ± 60	4.430	1072 ± 167
4.240	426 ± 56	4.320	417 ± 85	4.440	322 ± 102
4.243	445 ± 53	4.330	258 ± 88	4.450	554 ± 129
4.245	364 ± 47	4.340	307 ± 94	4.460	708 ± 0
4.248	569 ± 57	4.350	310 ± 90	4.480	197 ± 87
4.250	651 ± 66	4.360	277 ± 79	4.500	475 ± 134
4.255	620 ± 60	4.370	505 ± 97	4.520	616 ± 125
4.260	538 ± 55	4.380	329 ± 92	4.540	94 ± 69
4.265	762 ± 67	4.390	287 ± 88	4.550	304 ± 110
4.270	473 ± 56	4.395	396 ± 122	4.560	238 ± 135
4.275	649 ± 70	4.400	488 ± 116	4.570	517 ± 117
4.280	428 ± 57	4.410	687 ± 140	4.580	495 ± 134
4.285	862 ± 78	4.420	328 ± 96	4.590	308 ± 266
4.290	476 ± 63	4.425	335 ± 85	4.260	440 ± 40

Table 13: Dr. Wang Liangliang measured Born cross section of process $e^+e^- \to D_s^{*+}D_s^{*-}$ by using R-scan and XYZ data. The results colored in red are induced by XYZ data.

$\sqrt{s}$ (GeV)	σ (pb)	$\sqrt{s}$ (GeV)	σ (pb)	$\sqrt{s}$ (GeV)	σ (pb)
4.230	64 ± 23	4.330	96 ± 42	4.520	81 ± 49
4.235	275 ± 45	4.340	36 ± 36	4.540	148 ± 45
4.240	254 ± 52	4.350	26 ± 36	4.550	179 ± 45
4.243	412 ± 58	4.360	21 ± 44	4.560	107 ± 42
4.245	322 ± 55	4.370	1 ± 42	4.570	195 ± 50
4.248	408 ± 56	4.380	44 ± 44	4.580	117 ± 42
4.250	522 ± 64	4.390	156 ± 59	4.590	117 ± 48
4.255	374 ± 59	4.395	155 ± 57	4.226	36 ± 5
4.260	514 ± 62	4.400	192 ± 66	4.24160	461 ± 20
4.265	566 ± 66	4.410	325 ± 78	4.25797	541 ± 5
4.270	454 ± 61	4.420	392 ± 73	4.30790	227 ± 20
4.275	404 ± 61	4.425	365 ± 71	4.35820	35 ± 5
4.280	361 ± 59	4.430	288 ± 70	4.38740	145 ± 20
4.285	442 ± 62	4.440	425 ± 71	4.41558	397 ± 5
4.290	430 ± 61	4.450	283 ± 63	4.46706	262 ± 17
4.300	252 ± 55	4.460	320 ± 60	4.52714	121 ± 15
4.310	150 ± 47	4.480	146 ± 50	4.57450	126 ± 20
4.320	25 ± 24	4.500	160 ± 54	4.59953	140 ± 5

The Born cross section line-shape measured by BESIII as well as CLEO-c collaboration are shown in Figure 30.

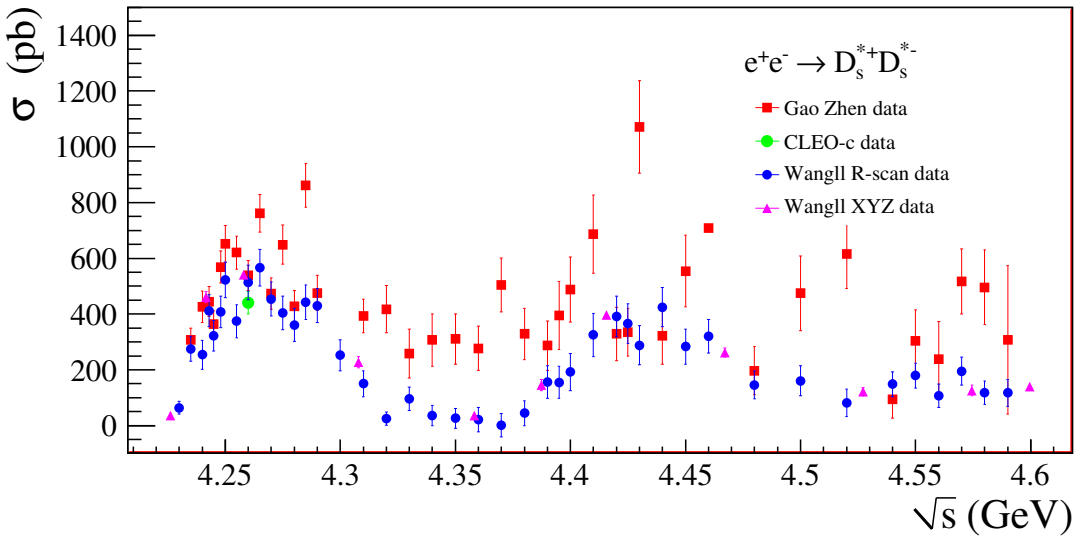

Figure 30: The Born cross section line-shape of process $e^+e^- \to D_s^{*+}D_s^{*-}$.

This channel is not implemented in the ConExc generator. We will consider it in new version of ConExc. The smooth cross section line-shape of process $e^+e^- \to D_s^{*+}D_s^{*-}$ will be obtained by fitting the BESIII data, as shown in Figure 30. This figure also show the comparison between measurements of Dr. Gao Zhen and Dr. Wang Liangliang. We can conclude that these two measurements consistent with each other within uncertainty.

In addition, Belle collaboration also measured the dressed cross section of process $e^+e^- \to D_s^{*+}D_s^{*-}$, as shown in Figure 31. It is hard to say whether the result of Belle is consistence with BESIII due to the large uncertainty in Belle's cross section.

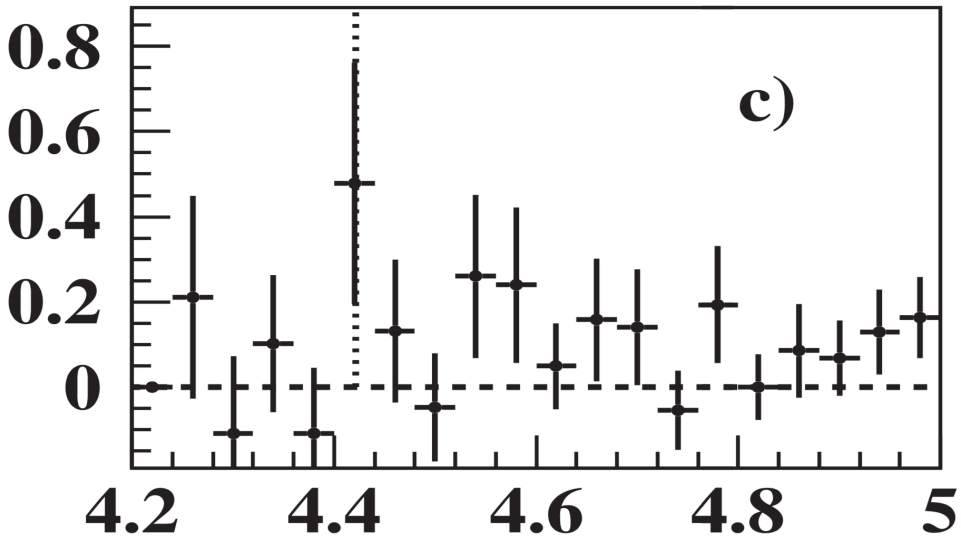

Figure 31: The dressed cross section of process $e^+e^- \to D_s^{*+}D_s^{*-}$, which is measured by Belle collaboration.

9.2 the phenomenological fit

We performed the phenomenological fit of Dr. Wang Liangliang data to obtain the smooth and continuum line-shape of $e^+e^- \to D_s^{*+}D_s^{*-}$. Figure 32 gives the fit result and Figure 33 is corresponding curve.

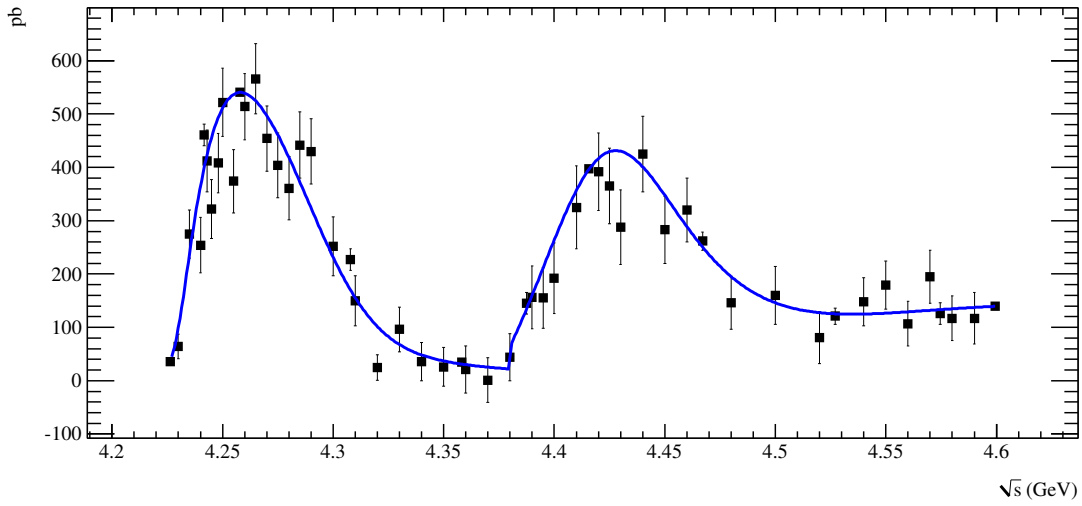

Figure 32: The fit result of Born cross section data of process $e^+e^- \to D_s^{*+}D_s^{*-}$ measured by Dr. Wang Liangliang.

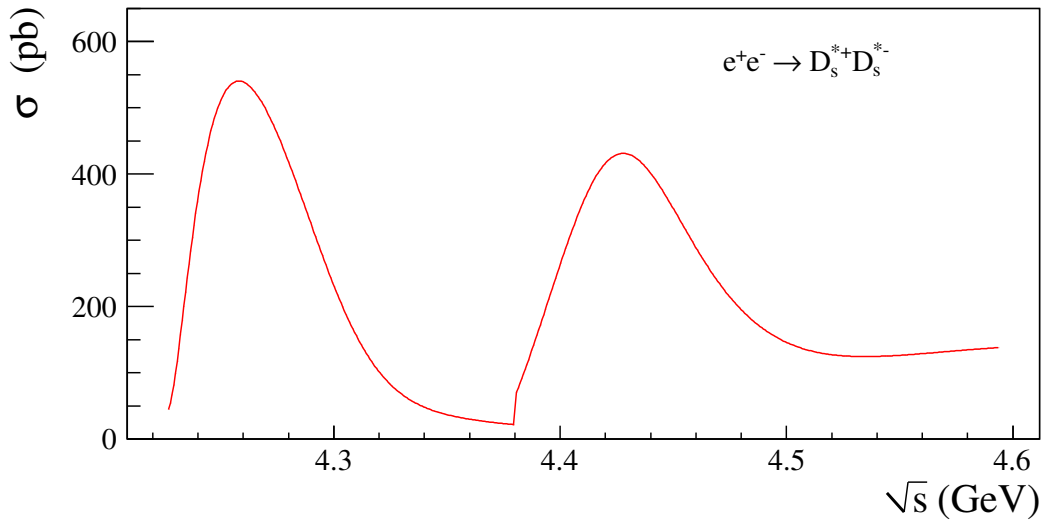

Figure 33: The fit curve of Born cross section data of process $e^+e^- \to D_s^{*+}D_s^{*-}$ measured by Dr. Wang Liangliang.

10 $e^+e^- \to D_2^*(2460)\bar{D}$

This channel is measured by Belle and BESIII collaborations but with different way.

10.1 BESIII result

BESIII analysis provided a very preliminary result of process $e^+e^- \to D_2^*(2460)\bar{D} \to D^0D^-\pi^+ + c.c$ by using R-scan and XYZ data together. In this measurement, the simulation is performed using KKMC and EVTGEN. In KKMC, the process $e^+e^- \to \psi(4415)$ is simulated, while in EVTGEN, the process $\psi(4415) \to D_2^*(2460)\bar{D}$ and the subsequence decay $D_2^*(2460) \to D\pi$ are simulated with corresponding branching fraction assigned to be 100%. Note that BESIII analysis included the charge-conjugation and isospin-conjugation modes: $e^+e^- \to D_2^{*+}(2460)D^-$, $e^+e^- \to D_2^{*-}(2460)D^+$, and $e^+e^- \to D_2^{*0}(2460)\bar{D}^0$, $e^+e^- \to \bar{D}_2^{*0}(2460)D^0$. In addition, this analysis eliminated the continuum contribution of process $e^+e^- \to D^0D^-\pi^+$ and its charge-conjugation modes. We have already know that:

$$D_2^{*0}(2460) \to D^+\pi^-, \quad \bar{D}_2^{*0}(2460) \to D^-\pi^+, \quad D_2^{*+}(2460) \to D^0\pi^+, \quad D_2^{*-}(2460) \to \bar{D}^0\pi^-,$$

we can obtain that

$$e^+e^- \to D_2^{*0}(2460)\bar{D}^0 \to \bar{D}^0D^+\pi^-, \quad e^+e^- \to \bar{D}_2^{*0}(2460)D^0 \to D^0D^-\pi^+,$$

$$e^+e^- \to D_2^{*+}(2460)D^- \to D^0D^-\pi^+, \quad e^+e^- \to D_2^{*-}(2460)D^+ \to \bar{D}^0D^+\pi^-.$$

Note that the isospin-conjugation mode

$$e^+e^- \to D^0\bar{D}\pi^0, \quad e^+e^- \to D^+D^-\pi^0$$

are not touched in this BESIII analysis.

Table 14 lists the measured results and Figure 34 shows the line-shape.

Table 14: The measured Born cross section of process $e^+e^- \to D_2^*(2460)\bar{D} \to D^0D^-\pi^+ + c.c$, where the uncertainty is total uncertainty.

$\sqrt{s}$ (GeV)	σ (pb)	$\sqrt{s}$ (GeV)	σ (pb)	$\sqrt{s}$ (GeV)	σ (pb)
4.340	96 ± 31	4.425	555 ± 71	4.540	125 ± 45
4.350	105 ± 28	4.430	734 ± 89	4.550	52 ± 46
4.360	232 ± 18	4.440	603 ± 72	4.560	57 ± 51
4.370	307 ± 43	4.450	499 ± 66	4.570	139 ± 48
4.380	417 ± 54	4.460	372 ± 59	4.575	122 ± 22
4.390	548 ± 45	4.470	338 ± 28	4.580	110 ± 48
4.395	506 ± 64	4.480	141 ± 49	4.590	78 ± 48
4.400	606 ± 72	4.500	232 ± 55	4.600	102 ± 10
4.410	640 ± 79	4.520	111 ± 50		
4.420	673 ± 48	4.530	147 ± 17		

It is necessary to point out that

$$\sigma^B(e^+e^- \to D_2^*(2460)D) \neq \sigma^B(e^+e^- \to D_2^*(2460)D \to D^0D^-\pi^+ + c.c.)$$

This is because $\mathcal{B}(D_2^*(2460) \to D\pi) \neq 100\%$. The particle $D_2^*(2460)$ can also decay into other modes, which are not employed to reconstruct the $D_2^*(2460)$ in this analysis. Therefore, the Born cross section of process $e^+e^- \to D_2^*(2460)D \to D^0D^-\pi^+ + c.c.$ is a part of that of $e^+e^- \to D_2^*(2460)D$, the correct interpretation takes the form

$$\sigma^B(e^+e^- \to D_2^*(2460)D) = \sigma^B(e^+e^- \to D_2^*(2460)D \to D^0D^-\pi^+ + c.c.)/\mathcal{B}(D_2^*(2460) \to D\pi).$$

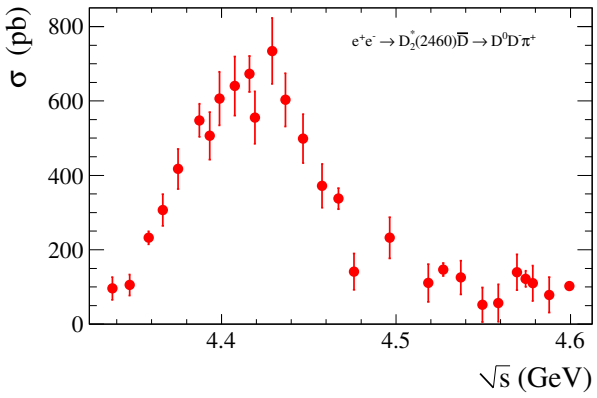

Figure 34: The Born cross section line-shape of process $e^+e^- \to D_2^*(2460)\bar{D} \to D^0D^-\pi^+ + c.c.$.

In addition, the authors also measured the continuum process $e^+e^- \to D^0D^-\pi^+ + c.c.$, as listed in Table 15 and Figure 35.

Table 15: The measured Born cross section of process $e^+e^- \to D^0D^-\pi^+ + c.c.$, where the first uncertainty is statistical and second is systematic.

$\sqrt{s}$ (GeV)	σ (pb)	$\sqrt{s}$ (GeV)	σ (pb)	$\sqrt{s}$ (GeV)	σ (pb)
4.009	59 ± 5	4.410	114 ± 90	4.530	49 ± 21
4.230	50 ± 6	4.420	54 ± 8	4.540	-6 ± 70
4.260	31 ± 6	4.425	80 ± 87	4.550	96 ± 76
4.340	97 ± 58	4.430	101 ± 93	4.560	171 ± 81
4.350	164 ± 65	4.440	39 ± 85	4.570	-63 ± 73
4.360	109 ± 11	4.450	-4 ± 84	4.575	39 ± 31
4.370	16 ± 68	4.460	214 ± 86	4.580	122 ± 78
4.380	44 ± 73	4.470	71 ± 23	4.590	32 ± 70
4.390	73 ± 32	4.480	-36 ± 79	4.600	63 ± 10
4.395	33 ± 79	4.500	-7 ± 81		
4.400	71 ± 85	4.520	148 ± 82		

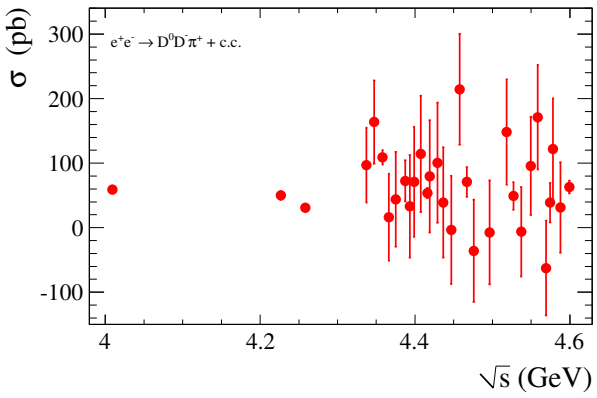

Figure 35: The Born cross section line-shape of continuum process $e^+e^- \to D^0D^-\pi^+ + c.c.$.

10.2 Belle result

Actually, Belle did not measure the cross section of the process $e^+e^- \to D_2^*(2460)D$ directly. They just measured the dressed cross section of process $e^+e^- \to D^0D^-\pi^+ + c.c$ inclusively. That is, the contribution from $D_2^*(2460) \to D\pi$ and continuum $e^+e^- \to D^0D^-\pi^+ + c.c$ processes. Note that in their measurement the contribution form $D^{*\pm}$ is vetoed. Figure 36 shown the measured results of Belle collaboration.

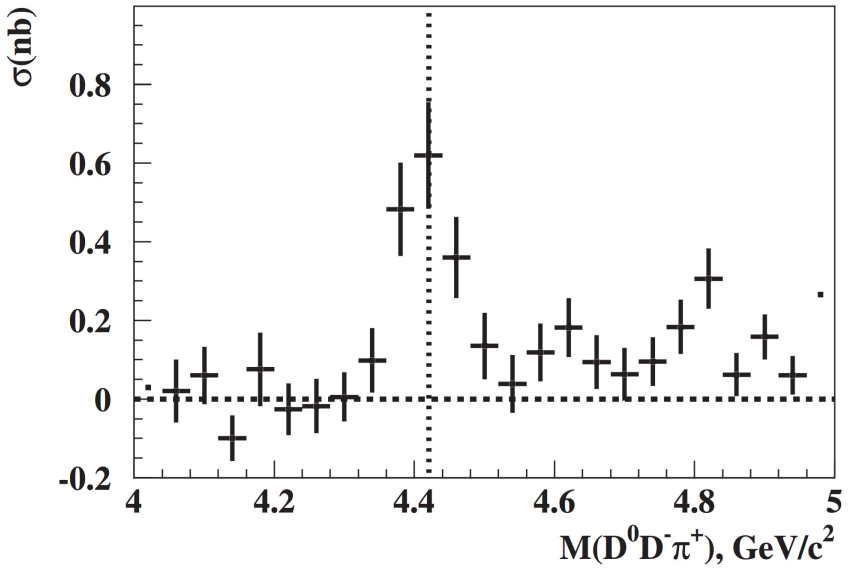

Figure 36: The dressed cross section line-shape of process $e^+e^- \to D^0D^-\pi^+ + c.c.$, where the contribution from the $e^+e^- \to D^-D^{*+}$ and $e^+e^- \to D^+D^{*-}$ are excluded. The measurement is performed by Belle Collaboration.

10.3 Implementing into the generator

Prof. Ronggang Ping had implemented this channel into the ConExc generator. The smooth line-shape is obtained by performing a phenomenological fit on Belle's data, as shown in Figure 37.

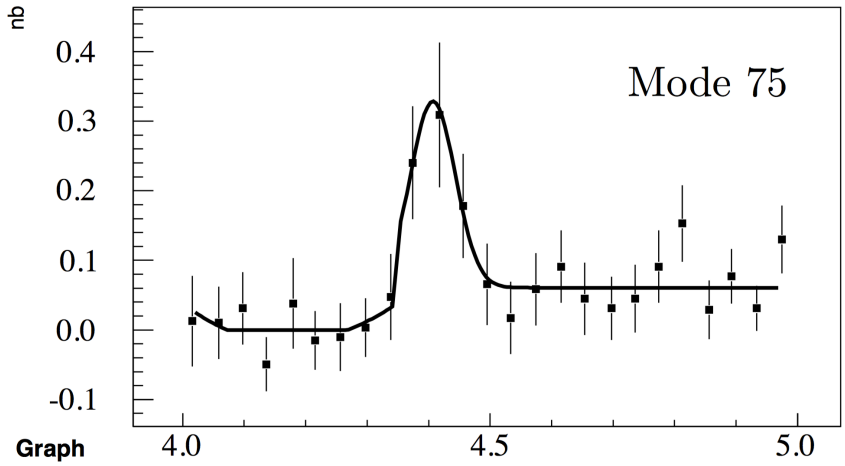

Figure 37: The phenomenological fit of cross section line-shape of process $e^+e^- \to D^0D^-\pi^+ + c.c.$, where the contribution from the $e^+e^- \to D^-D^{*+}$ and $e^+e^- \to D^+D^{*-}$ are excluded.

In the ConExc generator, the Born cross sections of processes $e^+e^- \to D^0D^-\pi^+$ and $e^+e^- \to \bar{D}^0D^+\pi^-$ are assigned to be a half of that of $e^+e^- \to D^0D^-\pi^+ + c.c.$, which is obtained by the fit performed based on Belle's measurement. This is reasonable that the cross section of charge-conjugation mode is equal. However, Prof. Ronggang Ping also implemented the isospin-conjugation processes of them: $e^+e^- \to D^0\bar{D}^0\pi^0$ and $e^+e^- \to D^+D^-\pi^0$, and their cross section are assigned to be the same as $e^+e^- \to D^0D^-\pi^+$.

Generally speaking, the Born cross sections of two isospin-conjugation modes are same at the same energy region, except at the threshold of these two modes due to the different masses of corresponding final state particles. For example, the Born cross section of $e^+e^- \to D^0\bar{D}^0$ and $e^+e^- \to D^+D^-$ are almost the same slightly above their thresholds. However, for different isospin-conjugation cases, we should also take the factor arisen from the isospin symmetry into consideration. For example, the cross section of $e^+e^- \to \pi^+\pi^- J/\psi$ is twice of that of isospin-conjugation process $e^+e^- \to \pi^0\pi^0 J/\psi$.

Regarding the processes $e^+e^- \to D^0D^-\pi^+$ and $e^+e^- \to D^0\bar{D}^0\pi^0$, we have

$$\left|\pi^+\right\rangle = |1,+1\rangle\,, \quad \left|\pi^0\right\rangle = |1,0\rangle\,, \quad \left|\pi^-\right\rangle = |1,-1\rangle$$

$$\left|D^0\right\rangle = \left|\frac{1}{2},-\frac{1}{2}\right\rangle, \quad \left|\bar{D}^0\right\rangle = \left|\frac{1}{2},+\frac{1}{2}\right\rangle, \quad \left|D^+\right\rangle = \left|\frac{1}{2},\frac{1}{2}\right\rangle, \quad \left|D^-\right\rangle = \left|\frac{1}{2},-\frac{1}{2}\right\rangle$$

Therefore,

$$\left|D^0\right\rangle\left|D^-\right\rangle\left|\pi^+\right\rangle = \left|\frac{1}{2},-\frac{1}{2}\right\rangle\left|\frac{1}{2},-\frac{1}{2}\right\rangle|1,+1\rangle$$

$$\left|\bar{D}^0\right\rangle\left|D^+\right\rangle\left|\pi^-\right\rangle = \left|\frac{1}{2},+\frac{1}{2}\right\rangle\left|\frac{1}{2},+\frac{1}{2}\right\rangle|1,-1\rangle$$

$$\left|D^0\right\rangle\left|\bar{D}^0\right\rangle\left|\pi^0\right\rangle = \left|\frac{1}{2},-\frac{1}{2}\right\rangle\left|\frac{1}{2},+\frac{1}{2}\right\rangle|1,0\rangle$$

$$\left|D^+\right\rangle\left|D^-\right\rangle\left|\pi^0\right\rangle = \left|\frac{1}{2},+\frac{1}{2}\right\rangle\left|\frac{1}{2},-\frac{1}{2}\right\rangle|1,0\rangle$$

In another hand, we have

$$\begin{aligned}
|0,0\rangle &= \frac{1}{\sqrt{3}}|1,+1\rangle|1,-1\rangle - \frac{1}{\sqrt{3}}|1,0\rangle|1,0\rangle + \frac{1}{\sqrt{3}}|1,-1\rangle|1,+1\rangle \\
&= \frac{1}{\sqrt{3}}\left(\left|\frac{1}{2},+\frac{1}{2}\right\rangle\left|\frac{1}{2},+\frac{1}{2}\right\rangle\right)|1,-1\rangle \\
&\quad - \frac{1}{\sqrt{3}}\left(\frac{1}{\sqrt{2}}\left|\frac{1}{2},+\frac{1}{2}\right\rangle\left|\frac{1}{2},-\frac{1}{2}\right\rangle + \frac{1}{\sqrt{2}}\left|\frac{1}{2},-\frac{1}{2}\right\rangle\left|\frac{1}{2},+\frac{1}{2}\right\rangle\right)|1,0\rangle \\
&\quad + \frac{1}{\sqrt{3}}\left(\left|\frac{1}{2},-\frac{1}{2}\right\rangle\left|\frac{1}{2},-\frac{1}{2}\right\rangle\right)|1,+1\rangle \\
&= \frac{1}{\sqrt{3}}\left|\frac{1}{2},+\frac{1}{2}\right\rangle\left|\frac{1}{2},+\frac{1}{2}\right\rangle|1,-1\rangle \\
&\quad - \frac{1}{\sqrt{6}}\left|\frac{1}{2},+\frac{1}{2}\right\rangle\left|\frac{1}{2},-\frac{1}{2}\right\rangle|1,0\rangle - \frac{1}{\sqrt{6}}\left|\frac{1}{2},-\frac{1}{2}\right\rangle\left|\frac{1}{2},+\frac{1}{2}\right\rangle|1,0\rangle \\
&\quad + \frac{1}{\sqrt{3}}\left|\frac{1}{2},-\frac{1}{2}\right\rangle\left|\frac{1}{2},-\frac{1}{2}\right\rangle|1,+1\rangle \\
&= \frac{1}{\sqrt{3}}\left|\bar{D}^0\right\rangle\left|D^+\right\rangle\left|\pi^-\right\rangle \\
&\quad - \frac{1}{\sqrt{6}}\left|D^+\right\rangle\left|D^-\right\rangle\left|\pi^0\right\rangle - \frac{1}{\sqrt{6}}\left|D^0\right\rangle\left|\bar{D}^0\right\rangle\left|\pi^0\right\rangle \\
&\quad + \frac{1}{\sqrt{3}}\left|D^0\right\rangle\left|D^-\right\rangle\left|\pi^+\right\rangle.
\end{aligned}$$

This immediately indicates that

$$\sigma^B(e^+e^- \to D^0\bar{D}^0\pi^0) \equiv \sigma^B(e^+e^- \to D^+D^-\pi^0) \equiv \frac{\sigma^B(e^+e^- \to D^0D^-\pi^+ + \bar{D}^0D^+\pi^-)}{4}$$

In summary, we should implement the charge- and isospin- conjugation modes of $e^+e^- \to D^0D^-\pi^+$ in the ConExc generator. They are $e^+e^- \to \bar{D}^0D^+\pi^-$, $e^+e^- \to D^0\bar{D}^0\pi^0$, and $e^+e^- \to D^+D^-\pi^0$. The smooth Born cross section line-shape of these modes are obtained by fitting Belle's measurement. At the same time, a $1/2$ factor should be multiplied when assigning the Born cross sections for processes $e^+e^- \to D^0\bar{D}^0\pi^0$ and $e^+e^- \to D^+D^-\pi^0$. In addition, the processes $e^+e^- \to D_2^*(2460)D$ should be excluded in LUNDA generator.

11 $e^+e^- \to D^0D^{*-}\pi^+$

11.1 the cross section data

BESIII collaboration provided a more precision measurement of process $e^+e^- \to D^0D^{*-}\pi^+$. In this measurement, the authors used both the R-scan data and the XYZ data. A partial reconstruction technique is implemented when reconstructing the final states $D^0D^{*-}\pi^+$, in which only one D^0 and a bachelor π^+ are reconstructed while the D^{*-} is not. The D^0 is reconstructed with $K^-\pi^+$. Note that the charge-conjugation final state $\bar{D}^0D^{*+}\pi^-$ is implied in this analysis.

The simulation is performed using KKMC and EVTGEN. In $e^+e^- \to D^0D^{*-}\pi^+$ process, the p-wave VSS model is used to generate the final states of $D^0D^{*-}\pi^+$. Note that the substructure of $D^0D^{*-}\pi^+$ is considered to estimate their influence on the detection efficiency.

In this analysis, the author extract the number of signal events by fitting the recoil mass spectrum of $D^0\pi^+$. Table 16 lists the measured result and Figure 38 shows the resulted Born cross section line-shape.

Table 16: The BESIII measured Born cross section of process $e^+e^- \to D^0D^{*-}\pi^+$ by using R-scan data and XYZ data (colored in blue), where the uncertainty is total unceratinty.

$\sqrt{s}$ (GeV)	σ (pb)	$\sqrt{s}$ (GeV)	σ (pb)	$\sqrt{s}$ (GeV)	σ (pb)
4.0474	19 ± 46	4.2374	242 ± 57	4.4274	665 ± 119
4.0524	-1 ± 38	4.2404	249 ± 54	4.4374	676 ± 119
4.0574	42 ± 33	4.2424	164 ± 47	4.4474	540 ± 111
4.0624	12 ± 26	4.2454	195 ± 52	4.4574	557 ± 104
4.0674	-24 ± 30	4.2474	156 ± 46	4.4774	449 ± 99
4.0774	36 ± 31	4.2524	128 ± 43	4.4974	494 ± 99
4.0874	32 ± 34	4.2574	133 ± 45	4.5174	464 ± 93
4.0974	76 ± 39	4.2624	130 ± 45	4.5374	619 ± 102
4.1074	28 ± 33	4.2674	165 ± 48	4.5474	472 ± 97
4.1174	28 ± 32	4.2724	147 ± 48	4.5574	502 ± 99
4.1274	40 ± 39	4.2774	188 ± 50	4.5674	547 ± 104
4.1374	97 ± 43	4.2824	156 ± 51	4.5774	486 ± 99
4.1424	112 ± 46	4.2874	123 ± 48	4.5874	527 ± 103
4.1474	47 ± 38	4.2974	229 ± 62	4.0855	40 ± 13
4.1574	156 ± 46	4.3074	240 ± 63	4.1886	172 ± 25
4.1674	53 ± 28	4.3174	329 ± 69	4.2077	265 ± 31
4.1774	148 ± 51	4.3274	358 ± 75	4.2171	242 ± 29
4.1874	190 ± 54	4.3374	456 ± 83	4.2263	250 ± 16
4.1924	212 ± 60	4.3474	459 ± 86	4.2417	199 ± 25
4.1974	193 ± 54	4.3574	264 ± 73	4.2580	152 ± 10
4.2004	243 ± 62	4.3674	570 ± 100	4.3079	268 ± 34
4.2034	222 ± 59	4.3774	659 ± 107	4.3583	489 ± 32
4.2074	244 ± 60	4.3874	876 ± 132	4.3874	665 ± 64
4.2124	303 ± 65	4.3924	665 ± 115	4.4156	698 ± 44
4.2174	222 ± 57	4.3974	688 ± 117	4.4671	557 ± 51
4.2224	245 ± 56	4.4074	647 ± 119	4.5271	480 ± 46
4.2274	284 ± 60	4.4174	683 ± 117	4.5745	407 ± 50
4.2324	250 ± 58	4.4224	856 ± 127	4.5995	454 ± 31

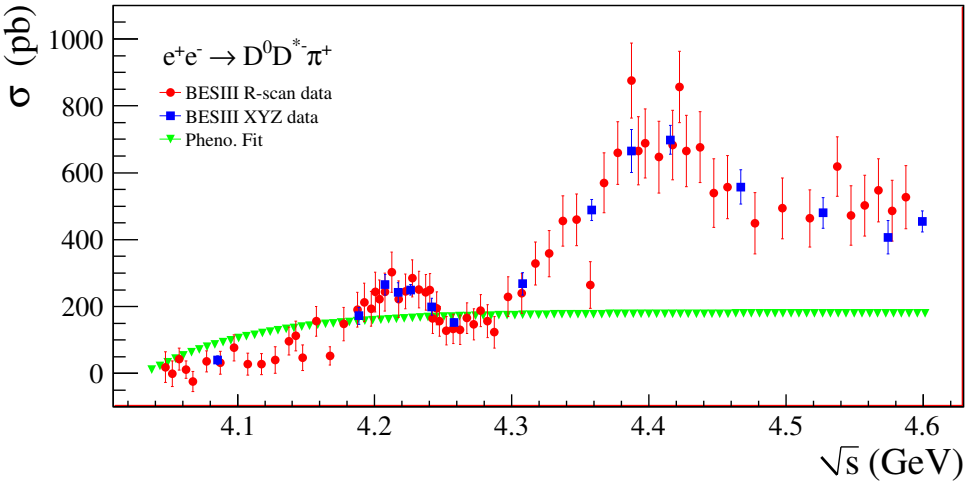

Figure 38: BESIII measured Born cross section line-shape of process $e^+e^- \to D^0D^{*-}\pi^+$, in which the charge-conjugation mode is included.

Belle collaboration also measured this mode by using the ISR technique. Figure 39 shows the measured result after a global scale due to the inclusion of the charge-conjugation channel $e^+e^- \to \bar{D}^0D^{*+}\pi^-$.

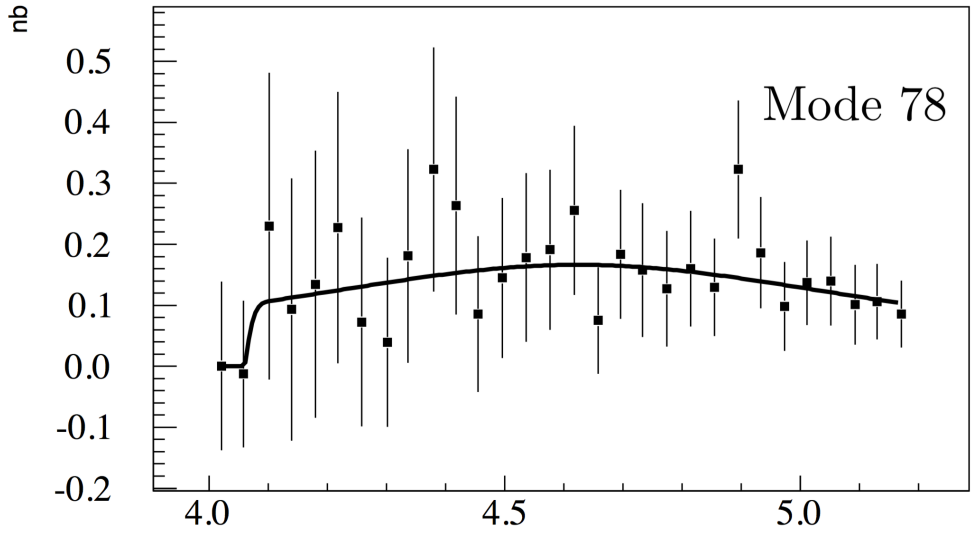

Figure 39: The Born cross section line-shape of process $e^+e^- \to D^0D^{*-}\pi^+$ measured by Belle collaboration, in which the charge-conjugation mode is included. The black solid line is a phenomenological fit performed for inclusive MC simulation.

Prof. Ping Ronggang performed a phenomenological fit for this channel, in order to obtain a smooth cross section line-shape for the ConExc generator, as shown by the black solid line in Figure 39 and the green triangles in Figure 38. We can concluded that the fit curve cannot fit the BESIII data. It is necessary that we impose a new fit.

11.2 the phenomenological fit

We performed the phenomenological fit of Dr. Wang Bin data to obtain the smooth and continuum line-shape of $e^+e^- \to D^0D^{*-}\pi^+$. Figure 40 gives the fit result and Figure 41 is corresponding curve.

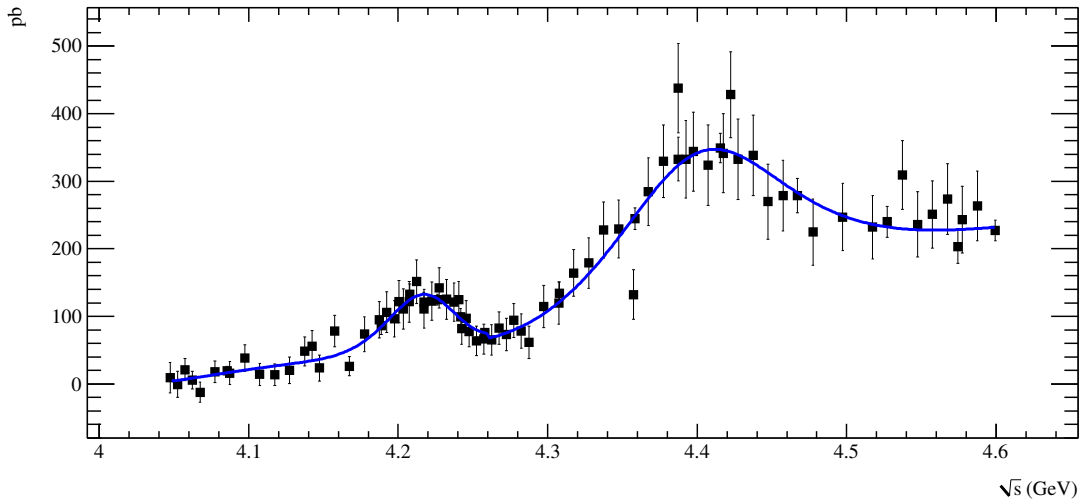

Figure 40: The fit result of Born cross section data of process $e^+e^- \to D^0D^{*-}\pi^+$ measured by Dr. Wang Bin.

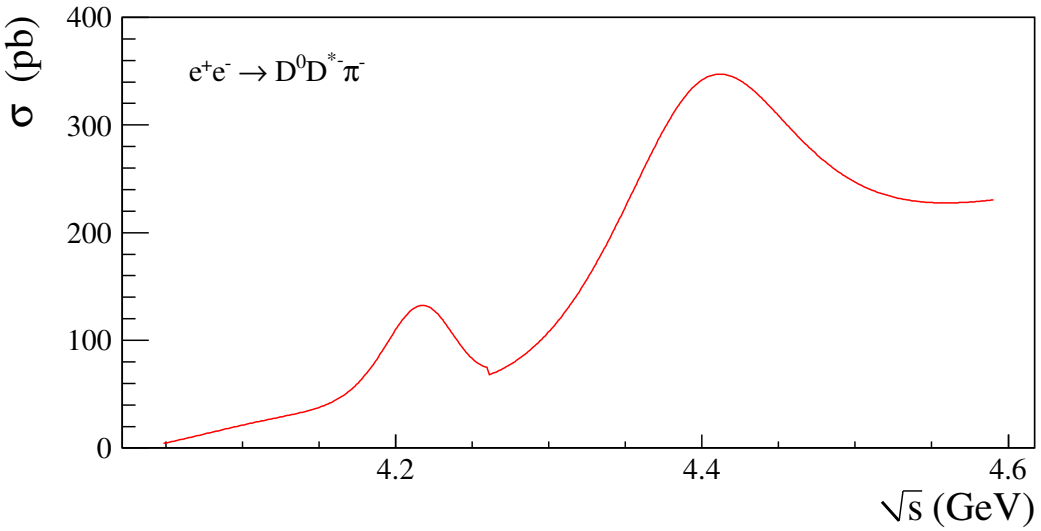

Figure 41: The fit curve of Born cross section data of process $e^+e^- \to D^0D^{*-}\pi^+$ measured by Dr. Wang Bin.

Note that the cross section channel $e^+e^- \to D^0D^{*-}\pi^+$ and $e^+e^- \to \bar{D}^0D^{*+}\pi^-$ are regarded as the same and assigned to be half of the $e^+e^- \to D^0D^{*-}\pi^+ + c.c.$, as we did in this fit procedure.

11.3 the isospin partners

At the end of this section, we will going to exploit all the charge- and isospin-conjugation channels of final state $D^0D^{*-}\pi^+$ and their cross section relations. Firstly, we have

$$\left|\pi^+\right\rangle = |1,+1\rangle\,,\quad \left|\pi^0\right\rangle = |1,0\rangle\,,\quad \left|\pi^-\right\rangle = |1,-1\rangle$$

$$\left|D^0\right\rangle = \left|\frac{1}{2},-\frac{1}{2}\right\rangle,\quad \left|\bar{D}^0\right\rangle = \left|\frac{1}{2},+\frac{1}{2}\right\rangle,\quad \left|D^+\right\rangle = \left|\frac{1}{2},\frac{1}{2}\right\rangle,\quad \left|D^-\right\rangle = \left|\frac{1}{2},-\frac{1}{2}\right\rangle$$

$$\left|D^{*0}\right\rangle = \left|\frac{1}{2},-\frac{1}{2}\right\rangle,\quad \left|\bar{D}^{*0}\right\rangle = \left|\frac{1}{2},+\frac{1}{2}\right\rangle,\quad \left|D^{*+}\right\rangle = \left|\frac{1}{2},\frac{1}{2}\right\rangle,\quad \left|D^{*-}\right\rangle = \left|\frac{1}{2},-\frac{1}{2}\right\rangle$$

We have already measured the processes:

$$e^+e^- \to D^0D^{*-}\pi^+,\quad \text{and}\quad e^+e^- \to \bar{D}^0D^{*+}\pi^-,$$

therefore we can immediately find their isospin partner channels:

$$e^+e^- \to D^{*0}D^-\pi^+,\quad \text{and}\quad e^+e^- \to \bar{D}^{*0}D^+\pi^-.$$

According to the discussion of last section, there are also channels:

$$e^+e^- \to \bar{D}^0D^{*0}\pi^0,\quad \text{and}\quad e^+e^- \to D^0\bar{D}^{*0}\pi^0,$$

and corresponding isospin partner modes

$$e^+e^- \to D^+D^{*-}\pi^0,\quad \text{and}\quad e^+e^- \to D^-D^{*+}\pi^0.$$

With the expansion

$$\begin{aligned}
|0,0\rangle &= \frac{1}{\sqrt{3}}|1,+1\rangle|1,-1\rangle - \frac{1}{\sqrt{3}}|1,0\rangle|1,0\rangle + \frac{1}{\sqrt{3}}|1,-1\rangle|1,+1\rangle \\
&= \frac{1}{\sqrt{3}}\left(\left|\frac{1}{2},+\frac{1}{2}\right\rangle\left|\frac{1}{2},+\frac{1}{2}\right\rangle\right)|1,-1\rangle \\
&\quad - \frac{1}{\sqrt{3}}\left(\frac{1}{\sqrt{2}}\left|\frac{1}{2},+\frac{1}{2}\right\rangle\left|\frac{1}{2},-\frac{1}{2}\right\rangle + \frac{1}{\sqrt{2}}\left|\frac{1}{2},-\frac{1}{2}\right\rangle\left|\frac{1}{2},+\frac{1}{2}\right\rangle\right)|1,0\rangle \\
&\quad + \frac{1}{\sqrt{3}}\left(\left|\frac{1}{2},-\frac{1}{2}\right\rangle\left|\frac{1}{2},-\frac{1}{2}\right\rangle\right)|1,+1\rangle\,.
\end{aligned}$$

We can conclude that

$$\sigma^B(e^+e^- \to D^{*0}D^-\pi^+) \equiv \sigma^B(e^+e^- \to \bar{D}^{*0}D^+\pi^-) \equiv \frac{\sigma^B(e^+e^- \to D^0D^{*-}\pi^+ + \bar{D}^0D^{*+}\pi^-)}{2}$$

$$\sigma^B(e^+e^- \to \bar{D}^0D^{*0}\pi^0) \equiv \sigma^B(e^+e^- \to D^0\bar{D}^{*0}\pi^0) \equiv \frac{\sigma^B(e^+e^- \to D^0D^{*-}\pi^+ + \bar{D}^0D^{*+}\pi^-)}{4}$$

$$\sigma^B(e^+e^- \to D^+D^{*-}\pi^0) \equiv \sigma^B(e^+e^- \to D^-D^{*+}\pi^0) \equiv \frac{\sigma^B(e^+e^- \to D^0D^{*-}\pi^+ + \bar{D}^0D^{*+}\pi^-)}{4}$$

In summary, we should implement the charge-conjugation and isospin partner modes of $e^+e^- \to D^0D^{*-}\pi^+$ in the ConExc generator. At the same time, a $1/2$ factor should be multiplied when assigning the Born cross sections for processes containing a π^0 in final states.

12 $e^+e^- \to \pi^+\pi^- J/\psi$

There are many measurements about this channel form BaBar, Belle, and BESIII collaboration. The fit of the cross section line-shape of this mode is quite abundant. In this section, we do not list the data of all the existed measurement in detail and just show corresponding plots instead.

Figure 42 show the first measured result of Belle collaboration.

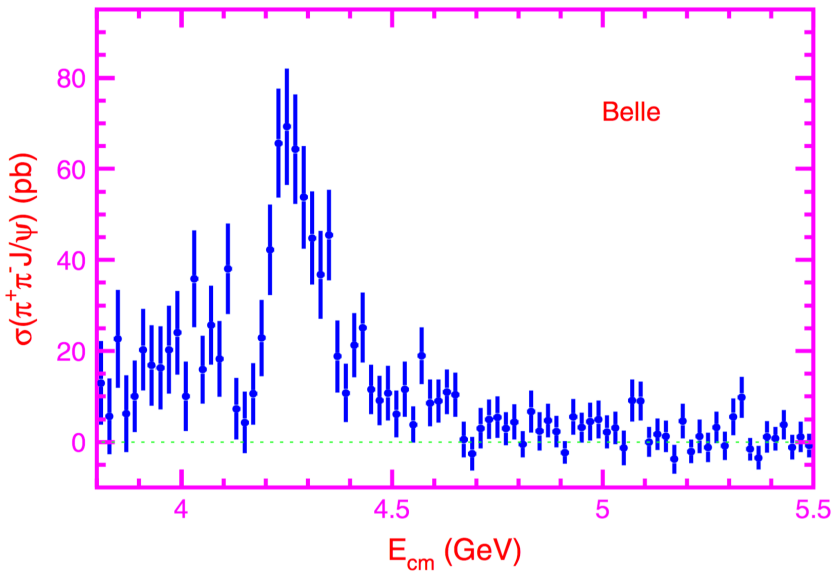

Figure 42: Belle collaboration measured dressed cross section line-shape of $e^+e^- \to \pi^+\pi^- J/\psi$.

Figure 43 show the updated measured result of Belle collaboration.

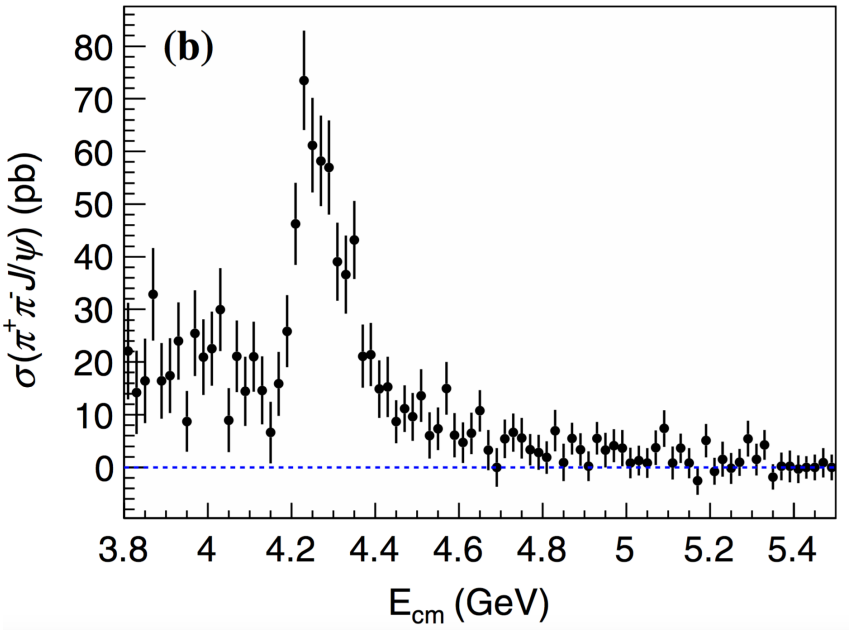

Figure 43: Belle's updated measurement of dressed cross section line-shape of $e^+e^- \to \pi^+\pi^- J/\psi$.

In Belle's two measurements of the $e^+e^- \to \pi^+\pi^- J/\psi$, a resonance around the c.m.s energy 4.0 GeV is claimed with the name $Y(4008)$. But neither the BaBar collaboration nor the BESIII measurement confirmed this resonance.

Figure 44 show the measured result of BaBar collaboration.

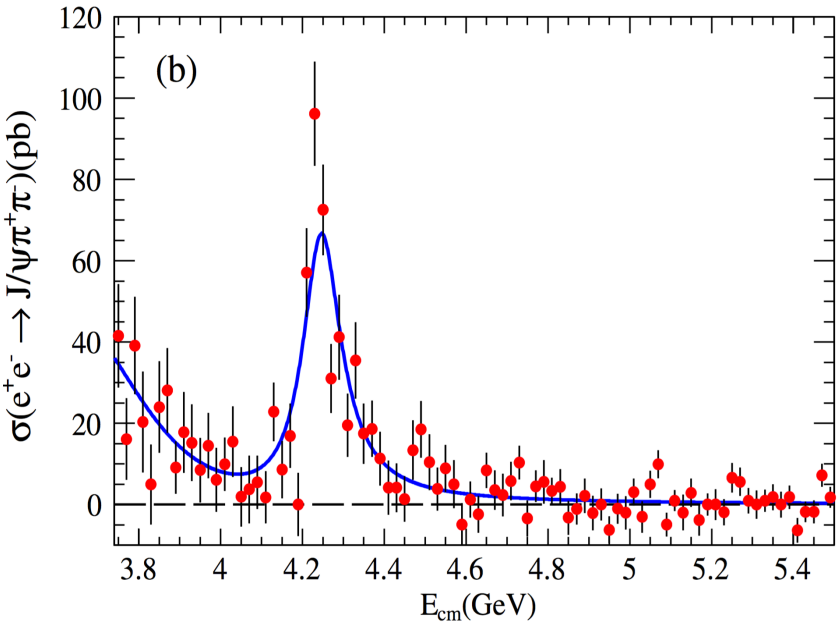

Figure 44: BaBar collaboration measured dressed cross section line-shape of $e^+e^- \to \pi^+\pi^- J/\psi$.

Figure 45 show the measured result of BESIII collaboration.

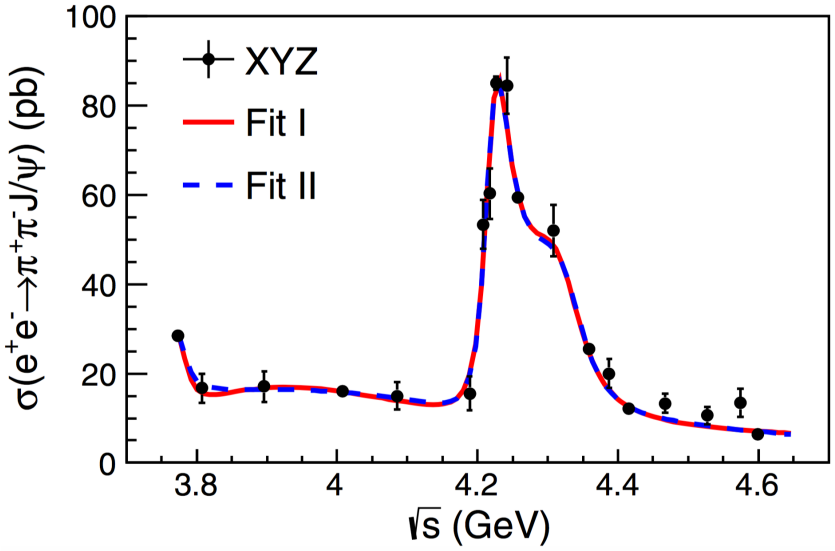

Figure 45: BESIII collaboration measured dressed cross section line-shape of $e^+e^- \to \pi^+\pi^- J/\psi$.

In the latest measurement performed by BESIII, the peak in the cross section line-shape of $e^+e^- \to \pi^+\pi^- J/\psi$ around 4.26 GeV, which is named as $Y(4260)$, is identified by the interference of the two resonances at 4220.0 MeV and 4320.0 MeV. The statistical significance of this resonance is estimated to be larger than 7.6σ.

The smooth Born cross section line-shape is obtained by fitting the Belle's first measured data, as shown in Figure 53.

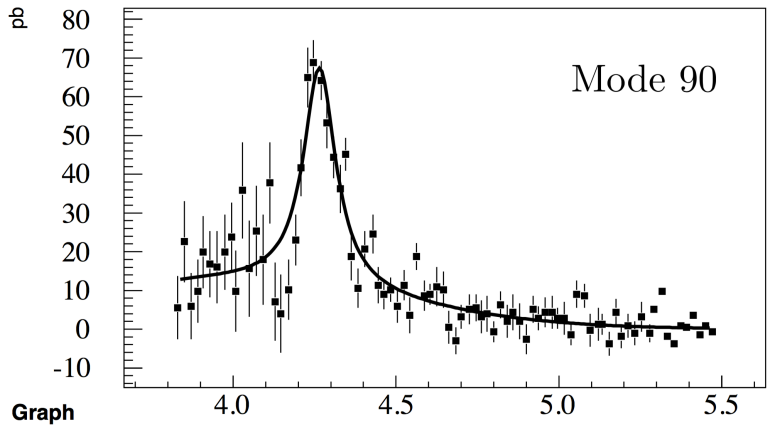

Figure 46: Prof. Ping Ronggang fitted cross section line-shape of $e^+e^- \to \pi^+\pi^- J/\psi$, in which the data is cited from Belle collaboration.

It is nature that we further talk about the cross section of process $e^+e^- \to \pi^0\pi^0 J/\psi$, since this mode is the isospin partner of $e^+e^- \to \pi^+\pi^- J/\psi$. Note that the isospin property of J/ψ is $|0,0\rangle$, therefore we can simply neglige the J/ψ in these two processes when calculating the isospin relations of them. For pions we have

$$\left|\pi^+\right\rangle = |1,+1\rangle\,, \quad \left|\pi^0\right\rangle = |1,0\rangle\,, \quad \left|\pi^-\right\rangle = |1,-1\rangle\,.$$

We can expand the initial states $|e^+e^-\rangle$ as following

$$\begin{aligned} |0,0\rangle &= \frac{1}{\sqrt{3}}\,|1,+1\rangle\,|1,-1\rangle - \frac{1}{\sqrt{3}}\,|1,0\rangle\,|1,0\rangle + \frac{1}{\sqrt{3}}\,|1,-1\rangle\,|1,+1\rangle \\ &= \frac{1}{\sqrt{3}}\left(\left|\pi^+\right\rangle\left|\pi^-\right\rangle - \left|\pi^0\right\rangle\left|\pi^0\right\rangle + \left|\pi^-\right\rangle\left|\pi^+\right\rangle\right) \end{aligned}$$

This immediately leads that

$$\sigma^B(e^+e^- \to \pi^0\pi^0 J/\psi) \equiv \frac{\sigma^B(e^+e^- \to \pi^+\pi^- J/\psi)}{2}$$

This relation can be proved by the measured result of the cross section $e^+e^- \to \pi^0\pi^0 J/\psi$, as shown in Figure 47, which is created by BESIII collaboration.

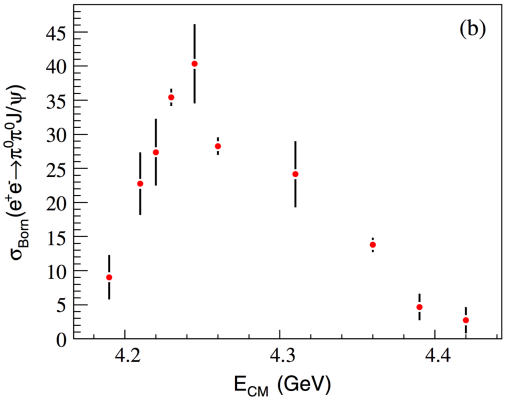

Figure 47: BESIII measured the Born cross section of process $e^+e^- \to \pi^0\pi^0 J/\psi$, in which the measurement only performed around 4.26 GeV.

As a result, we will simply assign the cross section line-shape of $e^+e^- \to \pi^0\pi^0 J/\psi$ to be the half of that of process $e^+e^- \to \pi^+\pi^- J/\psi$ as the input of generator ConExc.

13 $e^+e^- \to \pi^+\pi^-\psi(2S)$

This channel was firstly studied by BaBar with initial state radiation technique, in which the charmonium-like state $Y(4360)$ was observed and named. Belle collaboration then confirmed the existence of $Y(4360)$. BESIII collaboration also performed a similar measurement of the process $e^+e^- \to \pi^+\pi^-\psi(2S)$.

Figure 48 show the measured result of BaBar collaboration.

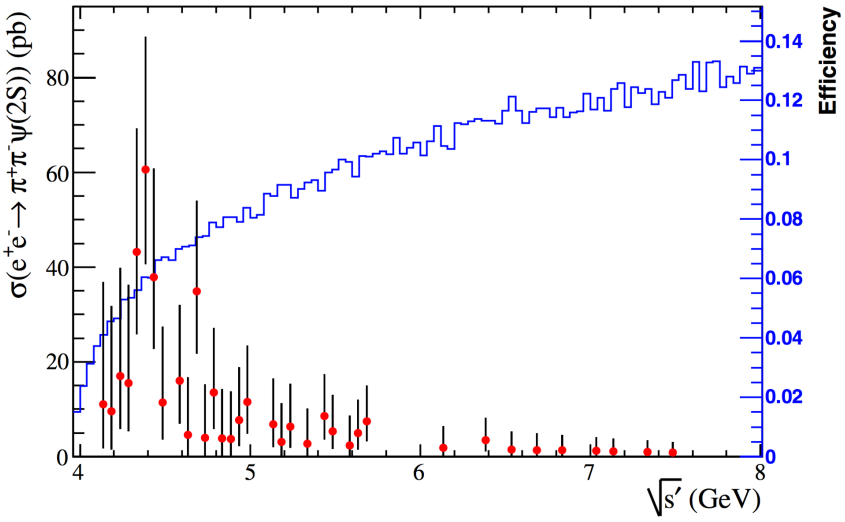

Figure 48: BaBar's first measurement of dressed cross section line-shape of $e^+e^- \to \pi^+\pi^-\psi(2S)$.

Figure 48 show the updated measurement of $e^+e^- \to \pi^+\pi^-\psi(2S)$ of BaBar collaboration.

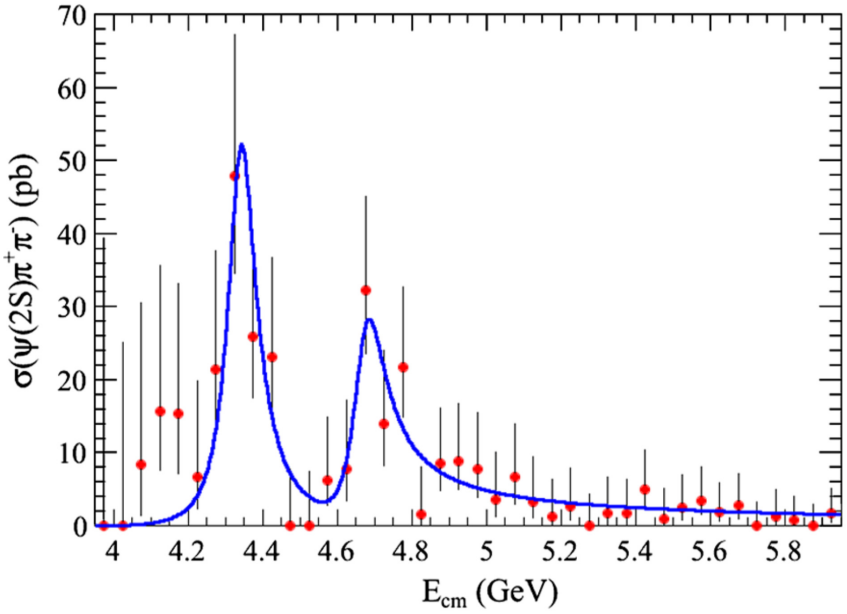

Figure 49: BaBar's updated measurement of dressed cross section of $e^+e^- \to \pi^+\pi^-\psi(2S)$.

In the updated measurement of BaBar collaboration, two resonances are used to describe the cross section of $e^+e^- \to \pi^+\pi^-\psi(2S)$, which are determined to be 4340 and 4669 MeV, respectively.

Figure 50 show the measured result of BaBar collaboration.

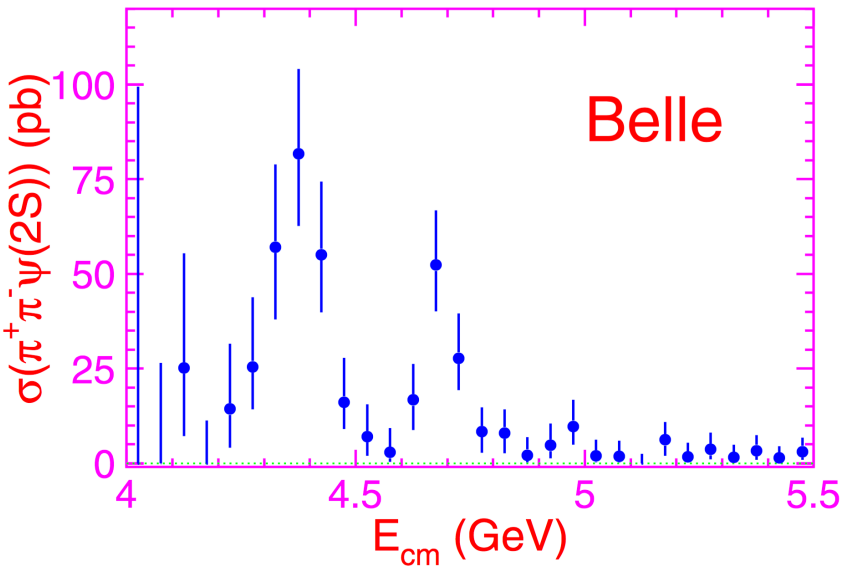

Figure 50: Belle's first measurement of dressed cross section line-shape of $e^+e^- \to \pi^+\pi^-\psi(2S)$.

Figure 50 show the updated measurement of $e^+e^- \to \pi^+\pi^-\psi(2S)$ of BaBar collaboration.

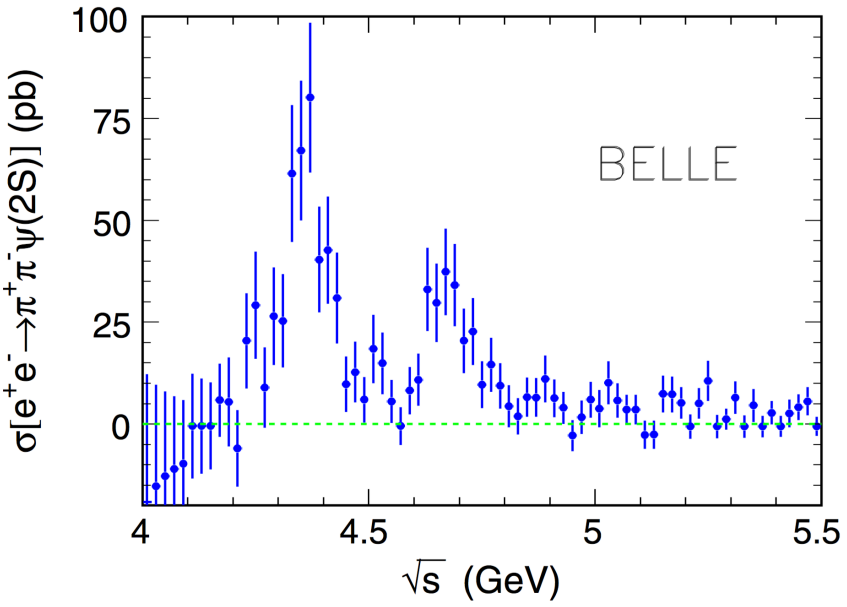

Figure 51: Belle's updated measurement of dressed cross section of $e^+e^- \to \pi^+\pi^-\psi(2S)$.

In the updated measurement of Belle collaboration, two resonances are used to describe the cross section of $e^+e^- \to \pi^+\pi^-\psi(2S)$, which are determined to be 4347 and 4652 MeV, respectively.

BESIII also studied this channel from 4.008 to 4.600 GeV, and confirmed the so-called $Y(4360)$ charmonium-like state, as shown in Figure 52. BESIII cannot tag the state $Y(4660)$ due to the c.m.s. energy limit of the accelerator BEPCII.

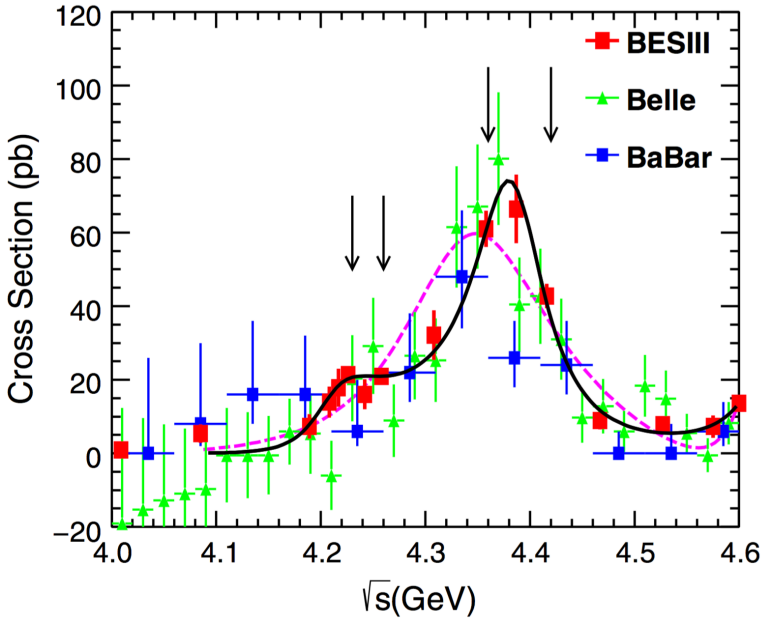

Figure 52: BESIII's measurement of Born cross section of $e^+e^- \to \pi^+\pi^-\psi(2S)$.

In generator ConExc, the smooth cross section line-shape of this channel is obtained by a phenomenological fit on Belle's data of first measurement. The fit result is shown in Figure 53. The fit quality is found to be good.

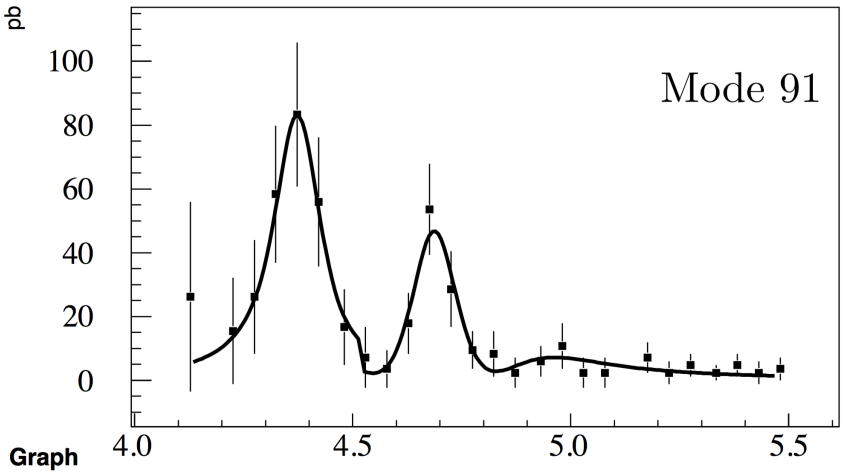

Figure 53: Prof. Ping Ronggang fitted cross section line-shape of $e^+e^- \to \pi^+\pi^-\psi(2S)$, in which the data is cited from Belle collaboration.

Similarly, the cross section line-shape of process $e^+e^- \to \pi^0\pi^0\psi(2S)$ is assigned to be the half of that of $e^+e^- \to \pi^+\pi^-\psi(2S)$ due to the isospin symmetry, which is verified by the BESIII measurement shown in Figure 54.

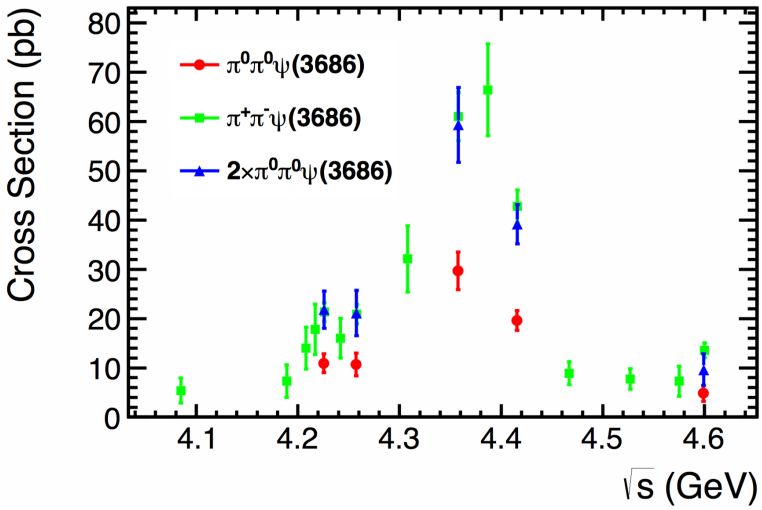

Figure 54: BESIII measured the Born cross section of process $e^+e^- \to \pi^0\pi^0\psi(2S)$, in which the measurement only performed below 4.60 GeV.

In summary, we implemented the processes $e^+e^- \to \pi^+\pi^-\psi(2S)$ and $e^+e^- \to \pi^0\pi^0\psi(2S)$ by performing a phenomenological fit on Belle data. Note that a $1/2$ factor should be included when handle the cross section of $e^+e^- \to \pi^0\pi^0\psi(2S)$ due to the isospin symmetry.

14 $e^+e^- \to \eta J/\psi$

The cross section line-shape of this channel is measured by Belle collaboration, in which the two charmonium-like called $Y(4040)$ and $Y(4160)$ are fixed at 4039 and 4153 MeV, respectively. Figure 55 shows the line-shape of $e^+e^- \to \eta J/\psi$ measured by Belle collaboration.

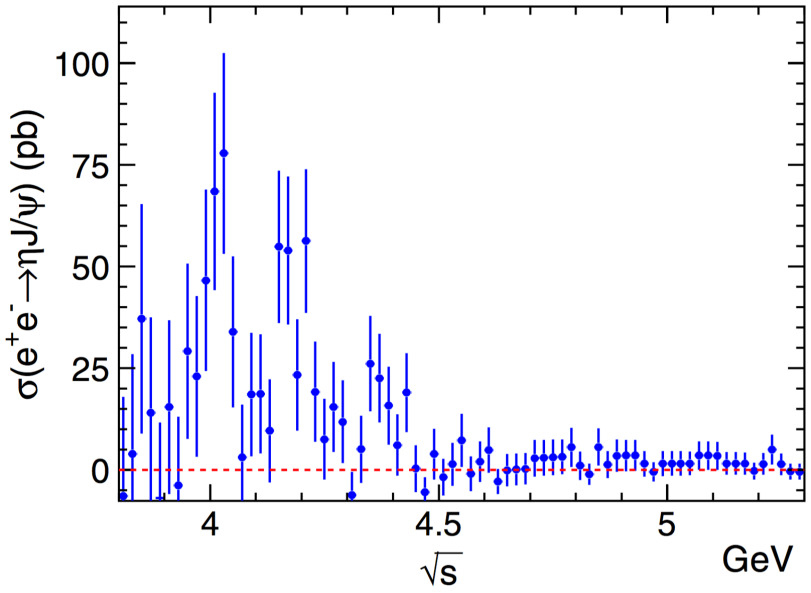

Figure 55: Belle's measurement of dressed cross section line-shape of $e^+e^- \to \eta J/\psi$.

A smooth cross section line-shape of this channel is obtained by performing a phenomenological fit on Belle's data, as shown in Figure 56.

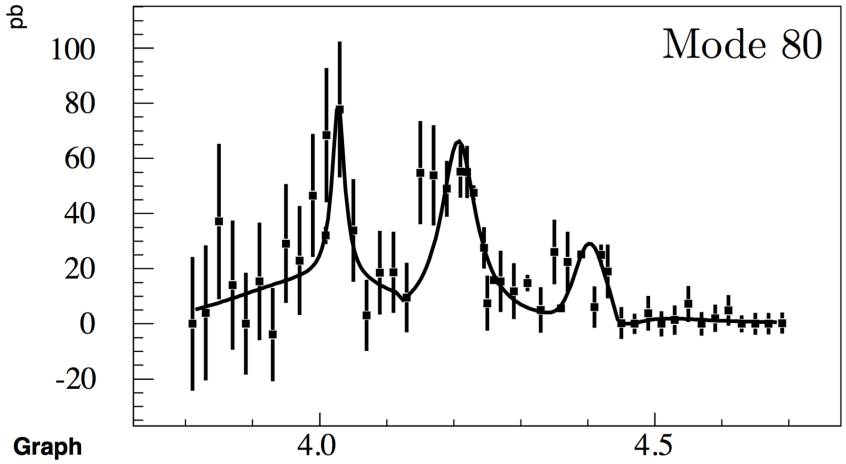

Figure 56: The input cross section line-shape of $e^+e^- \to \eta J/\psi$ for ConExc generator.

15 $e^+e^- \to K^+K^-J/\psi$

The cross section line-shape of this channel is measured by Belle collaboration, and no significant signal of $Y(4260) \to K^+K^-J/\psi$ is observed. Figure 57 shows the line-shape of $e^+e^- \to K^+K^-J/\psi$ measured by Belle collaboration.

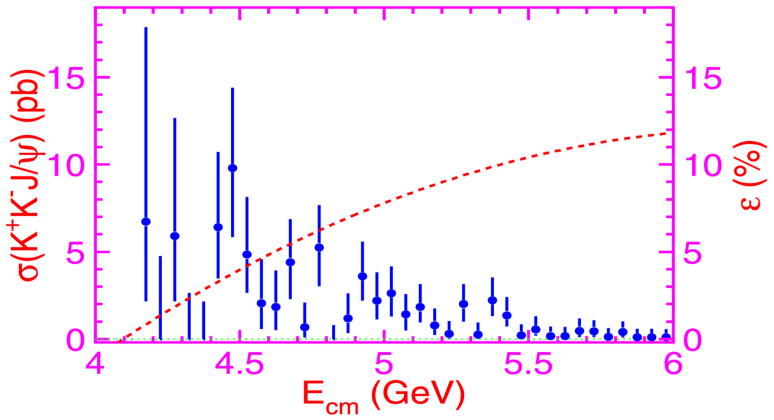

Figure 57: Belle's measurement of dressed cross section line-shape of $e^+e^- \to K^+K^-J/\psi$.

A smooth cross section line-shape of this channel is obtained by performing a phenomenological fit on Belle's data, as shown in Figure 58.

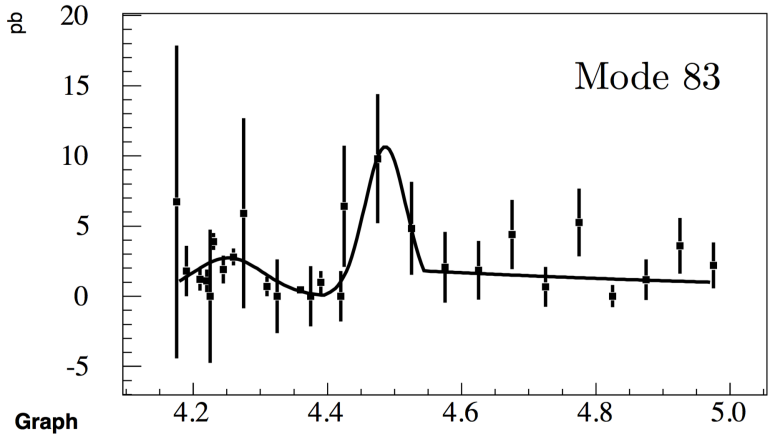

Figure 58: The input cross section line-shape of $e^+e^- \to K^+K^-J/\psi$ for ConExc generator.

In this analysis, the channel $e^+e^- \to K^0_S K^0_S J/\psi$ is also considered but not measured due to the limit of the statistics. However, a ratio of the average cross section between the neutral and charged modes are presented as

$$\frac{\bar{\sigma}_{K^0_S K^0_S J/\psi}}{\bar{\sigma}_{K^+K^-J/\psi}} = 0.6^{+0.5}_{-0.4},$$

which is in agreement with the expectation (1/2) of the isospin symmetry.

Therefore, in generator ConExc, we implemented the channel $e^+e^- \to K^+K^-J/\psi$ and $e^+e^- \to K^0_S K^0_S J/\psi$ by using the data measured by Belle, and a factor 1/2 due to the isospin-symmetry is included when assigning the cross section lien-shape of the $e^+e^- \to K^0_S K^0_S J/\psi$.

In addition, BESIII collaboration is also measured this channel using BESIII XYZ data, as shown in Figure 59.

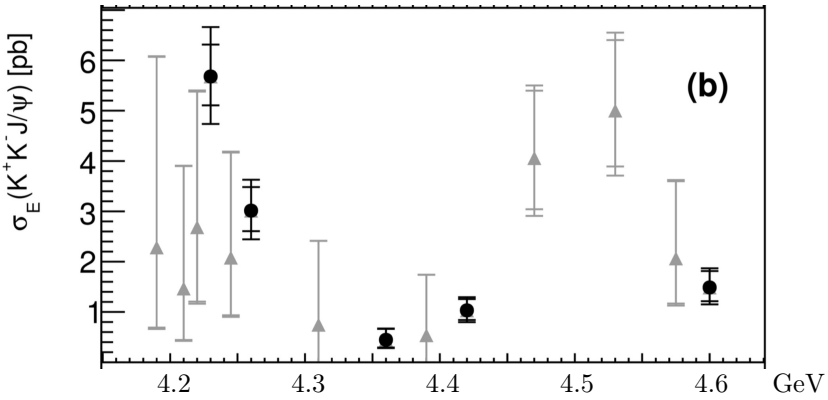

Figure 59: BESIII's measurement of Born cross section line-shape of $e^+e^- \to K^+K^-J/\psi$.

Due to the large statistics of XYZ data, it is also possible that BESIII measure the cross section of $e^+e^- \to K^0_S K^0_S J/\psi$. Figure 60 shows the results.

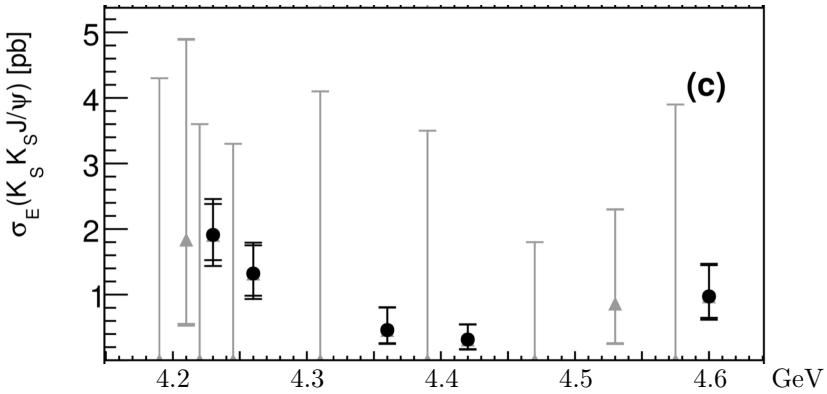

Figure 60: BESIII's measurement of Born cross section line-shape of $e^+e^- \to K^0_S K^0_S J/\psi$.

In addition, the isospin symmetry between K^+K^- and $K^0\bar{K}^0$ leads that

$$\sigma^B(e^+e^- \to K^0_S K^0_S J/\psi) \equiv \sigma^B(e^+e^- \to K^0_L K^0_L J/\psi) \equiv \frac{\sigma^B(e^+e^- \to K^0\bar{K}^0 J/\psi)}{2} \equiv \frac{\sigma^B(e^+e^- \to K^+K^- J/\psi)}{2}.$$

This fact is verified by BESIII analysis as shown in Figure 61.

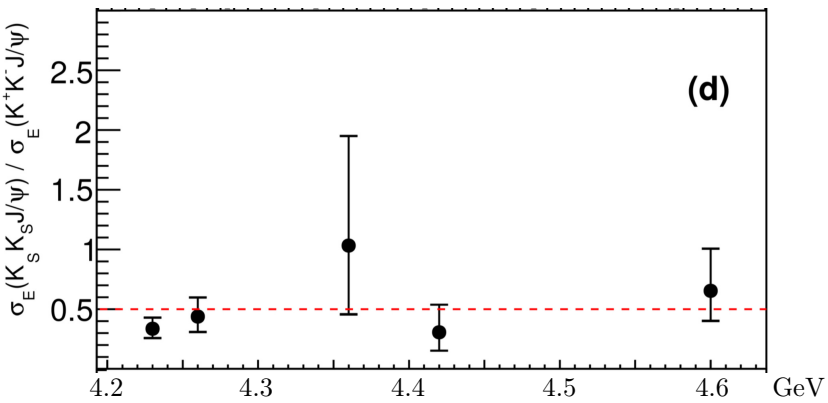

Figure 61: BESIII's measurement of Born cross section ratio between $e^+e^- \to K^0_S K^0_S J/\psi$ and $e^+e^- \to K^+K^-J/\psi$.

16 $e^+e^- \to \pi^+\pi^- h_c$

16.1 the cross section

BESIII collaboration measured this channel by using its XYZ data from 3.90 to 4.42 GeV for the first time, the measured result is shown in Figure 62.

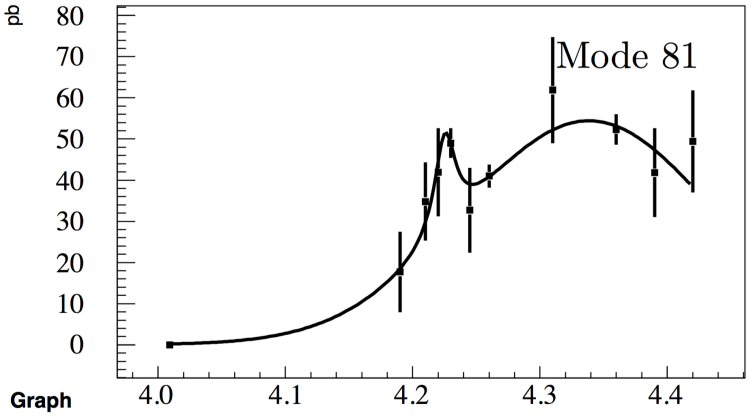

Figure 62: The input cross section line-shape of $e^+e^- \to \pi^+\pi^- h_c$ for ConExc generator, where the data is cited from BESIII collaboration.

These results are also used to obtaining the smooth input cross section for ConExc generator after a phenomenological fit, which is shown in Figure 62. After this measurement, BESIII collaboration performed their updated analysis of this channel. In the updated analysis, the cross section of process $e^+e^- \to \pi^+\pi^- h_c$ is measured from 3.896 to 4.600 GeV, as shown in Figure 63. In this analysis, two new charmonium-like states are evident as $Y(4220)$ and $Y(4390)$ at c.m.s 4218.4 and 4391.5 GeV, respectively.

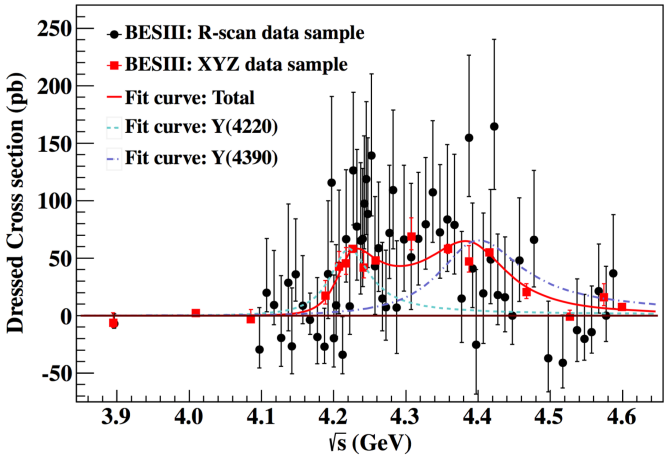

Figure 63: BESIII's updated measurement of cross section line-shape of $e^+e^- \to \pi^+\pi^- h_c$.

In this case, we need to update our phenomenological fit on this channel to obtain a better description of real data. Fortunately, the author of this analysis have already provided a good fit, which can be used directly.

Similarly, according to the isospin symmetry, the cross section of process $e^+e^- \to \pi^0\pi^0 h_c$ can also be determined:

$$\sigma^B(e^+e^- \to \pi^0\pi^0 h_c) \equiv \frac{\sigma^B(e^+e^- \to \pi^+\pi^- h_c)}{2}.$$

Therefore, in the generator ConExc, we can implement these two channels after assigning a $1/2$ factor to the neutral mode.

16.2 the phenomenological fit

Table 17: The measured Born cross section of process $e^+e^- \to \pi^+\pi^- h_c$ by using XYZ data. The uncertainties do not include contribution from the uncertainty of $\mathcal{B}(h_c \to \gamma\eta_c)$.

$\sqrt{s}$ (GeV)	σ (pb)	$\sqrt{s}$ (GeV)	σ (pb)	$\sqrt{s}$ (GeV)	σ (pb)	$\sqrt{s}$ (GeV)	σ (pb)
4.009	0 ± 5	4.220	42 ± 11	4.310	62 ± 14	4.470	19 ± 7
4.090	0 ± 13	4.230	50 ± 5	4.360	52 ± 6	4.530	-1 ± 5
4.190	18 ± 10	4.245	33 ± 11	4.390	42 ± 11	4.575	15 ± 11
4.210	35 ± 10	4.260	41 ± 5	4.420	49 ± 13	4.600	7 ± 2

We performed the phenomenological fit of BESIII data (listed in Table 17) to obtain the smooth and continuum line-shape of $e^+e^- \to \pi^+\pi^- h_c$. Figure 64 gives the fit result and Figure 65 is corresponding curve.

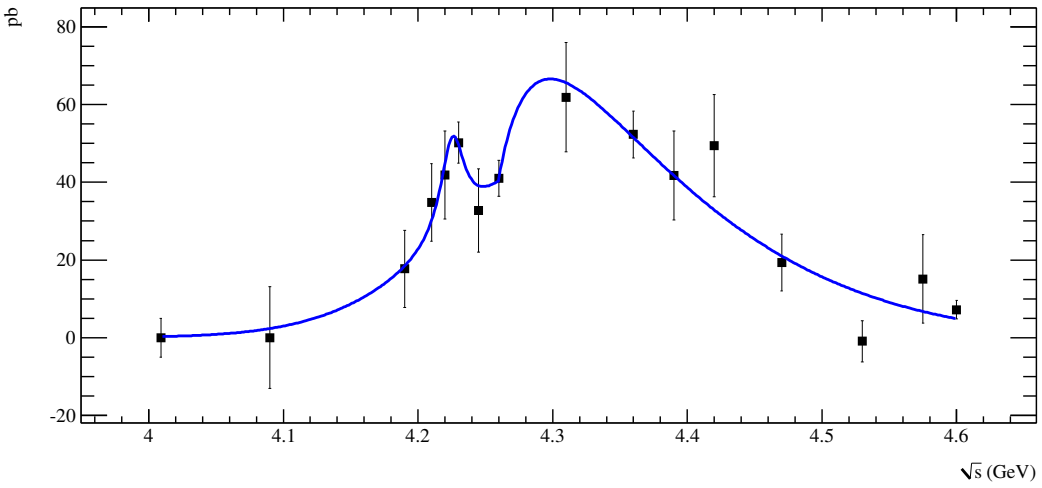

Figure 64: Fit result of Born cross section process $e^+e^- \to \pi^+\pi^- h_c$ measured by BESIII.

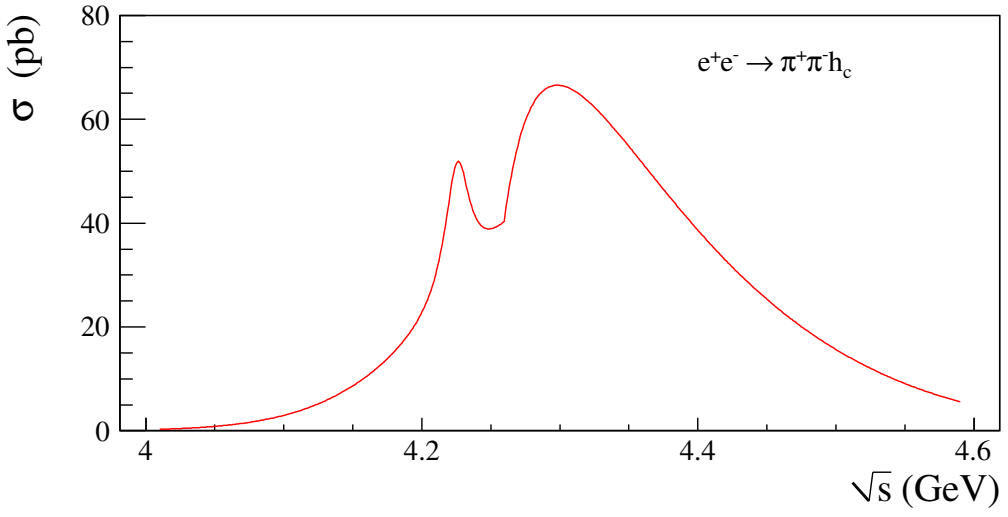

Figure 65: Fit curve of Born cross section process $e^+e^- \to \pi^+\pi^- h_c$ measured by BESIII.

17 $e^+e^- \to \Lambda_c^+ \bar{\Lambda}_c^-$

Belle collaboration measured the cross section line-shape of $e^+e^- \to \Lambda_c^+ \bar{\Lambda}_c^-$ from threshold to 5.4 GeV using the ISR technique, as shown in Figure 66.

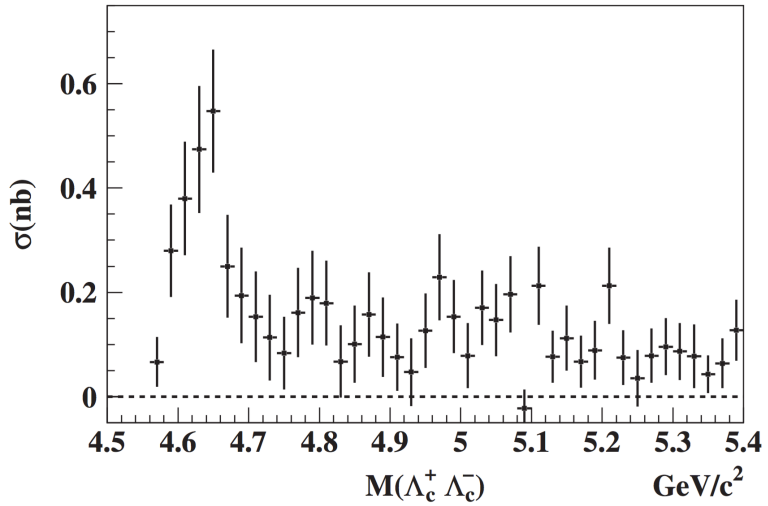

Figure 66: Belle's measurement of cross section line-shape of $e^+e^- \to \Lambda_c^+ \bar{\Lambda}_c^-$.

Recently, BESIII collaboration also performed a measurement of the $\Lambda_c^+ \bar{\Lambda}_c^-$ production cross section near the threshold. In this analysis, the enhanced cross section at the threshold is evidenced for the first time. Figure 67 shows the measured results. The measurement is limited by the energy scale of the accelerator BEPCII comparing with Belle', measurement.

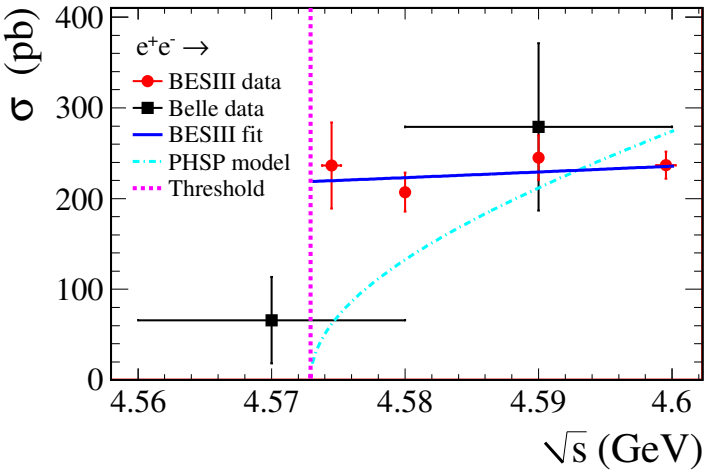

Figure 67: BESIII's measurement of cross section line-shape of $e^+e^- \to \Lambda_c^+ \bar{\Lambda}_c^-$ near its threshold.

To obtain a smooth input line-shape of ConExc generator, a phenomenological fit is performed after combining the data of BESIII and Belle. The fit result as well as the combined data is shown in Figure 68.

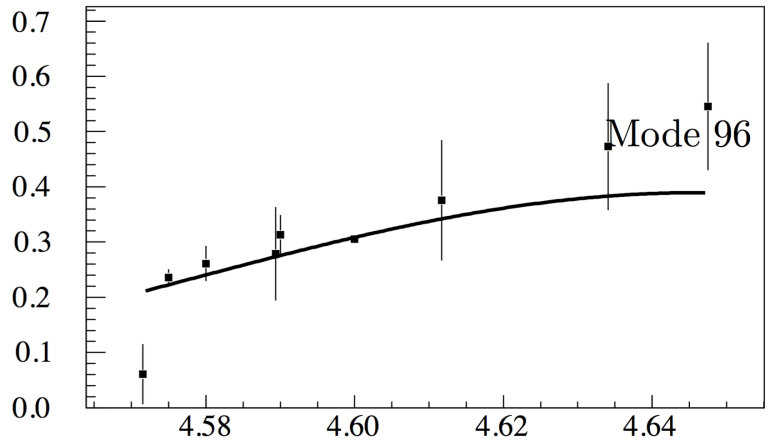

Figure 68: The phenomenological fit of cross section line-shape of $e^+e^- \to \Lambda_c^+\bar{\Lambda}_c^-$, in which the data is obtained by combining the results of Belle and BESIII.

We can conclude that the fit is good enough to describe the Born cross section of process $e^+e^- \to \Lambda_c^+\bar{\Lambda}_c^-$.